AN ABSTRACT OF THE THESIS OF

RAYMOND A. HASKINS for the degree of MASTER OF SCIENCE in Electrical and Computer Engineering presented on August 12, 1976

Title: ANALYSIS AND SIMULATION OF A VARIABLE SPEED INDUCTION MOTOR

Redacted for Privacy

Abstract approved: Owen D. Osborne

A model of a squirrel cage induction machine, d.c.-link power supply and centrifugal pump is developed and used in the design and evaluation of a perturbation feedback control system for a sewage pumping station. A comparison of the simulation model of the induction machine and a laboratory machine to a sinusoidal supply voltage is presented. The control system gains are determined using the steady state solution of the discrete Ricatti equation developed in linear quadratic optimal control theory. A simulation of the system is developed and used to demonstrate the open loop starting characteristic of the system, evaluate the convergence properties of the gain calculations and demonstrate the stability of the resulting feedback controller. Open and closed loop system pole placement is evaluated using transform methods. Simulation results show that the gain calculations converge

in five iterations on the first sample instant of closed loop operation, and subsequently converge in one iteration and that the closed loop system is stable. Evaluation of the closed loop system pole placement also indicates stability of the perturbation controller.

Analysis and Simulation of an Induction Motor

by

Raymond A. Haskins

A THESIS

submitted to

Oregon State University

in partial fulfillment of
the requirements for the
degree of

Master of Science

June 1977

APPROVED:

Redacted for Privacy

Associate Professor of Electrical and Computer Engineering
in charge of major

Redacted for Privacy

Head of Department of Electrical and Computer Engineering

Redacted for Privacy

Dean of Graduate School

Date thesis is presented August 12, 1976

Typed by Lora Wixom/Typing for Raymond A. Haskins

ACKNOWLEDGMENT

The support of the faculty and staff of the Oregon State University Department of Electrical and Computer Engineering is gratefully acknowledged. The Statistics Department's cooperation in providing access to their computer terminals was helpful. Helpful discussions and motivation were provided by Mr. John Sewell of CH_2M-Hill and Mr. C. R. Faes of Jackson Rand Corporation. Substantial technical direction and active participation in the development and evaluation of the induction machine model was provided by Dr. G. C. Alexander. Dr. Owen D. Osborne's even handed administration of my program and this work was highly beneficial. Finally, the sense of humor, enthusiasm, and interest of my fellow students proved to be of significant aid; in particular, discussion with and the participation of Mike Drost is uncompensable.

The computer simulation and evaluation work reported herein was supported by Oregon State University under account number 758122.

TABLE OF CONTENTS

LIST OF ILLUSTRATIONS

LIST OF SYMBOLS

SYMBOL	DESCRIPTION	UNITS
A	Plant matrix	———
B	Input matrix	———
C	Output matrix	———
D	Viscous friction coefficient	N-m/(r/s)
F	Plant function	———
h_f	Friction head	m
h_p	Pump head	m
h_s	Static head	m
h	Well head	m
I	Value of cost function	———
i	Current vector	A
$i_{\alpha s}$	α-component of stator current	A
$i_{\gamma s}$	γ-component of stator current	A
$i_{\alpha r}$	α-component of rotor current	A
$i_{\gamma r}$	γ-component of rotor current	A
J	Moment of inertia	$Kg\text{-}m^2$
k_f	System friction head coefficient	$m/(m^3/s)$
k_h	Pump output head coefficient	$m/(r/s)^2$
k_t	Pump reaction torque coefficient	$N\text{-}m/(r/s)^2$
k_w	Reciprocal of well area	m^{-2}
L	Inductance matrix	H
l_m	Machine mutual inductance	H
l_r	Machine rotor inductance	H
l_s	Machine stator inductance	H
m	System fluid mass	kg

SYMBOL	DESCRIPTION	UNITS
n	Machine pole pairs	———
Q	State cost weighting matrix	———
q_1	System input flow	m^3/s
q_p	Pump output flow	m^3/s
R	Machine resistance matrix also control cost weighting matrix	ohm
r_r	Rotor resistance	ohms
r_s	Stator resistance	ohms
s	Complex variable	s^{-1}
T	Sample period	s
t	Time	s
t_e	Machine electromagnetic torque	N-m
t_p	Pump reaction torque	N-m
t_s	Supply voltage switching time	s
$\underline{u}$	Control vector	———
$\underline{u}_o$	Open loop control vector	———
$\underline{\delta u}$	Control vector perturbation	———
v	Machine input voltage vector	V
v_a	Stator phase a instantaneous voltage	V
v_b	Stator phase b instantaneous voltage	V
v_c	Stator phase c instantaneous voltage	V
v_d	d.c.-link output voltage	V
V_m	Amplitude of fundamental component supply voltage	V
v_α	α -component of stator voltage	V
v_γ	γ -component of stator voltage	V
$\underline{x}$	State vector	———
$\underline{x}_c$	Target state vector	———
$\underline{x}_o$	Open loop state vector	———
$\underline{\delta x}$	State vector perturbation	———

SYMBOL	DESCRIPTION	UNITS
$\underline{y}$	Output vector	———
z	Complex variable	———
θ	Supply voltage phase	
ϕ	State transition matrix	———
ψ	Control transition matrix	———
ω_m	Rotor Angular frequency	r/s
ω_s	Supply voltage fundamental frequency	r/s

ANALYSIS AND SIMULATION OF A VARIABLE SPEED INDUCTION MOTOR

I. THE RESEARCH PROBLEM

Introduction

Static frequency converters using thyristors provide a method for obtaining speed control of squirrel cage induction motors [1]. The attractiveness of these systems is due in part to the low cost and high reliability of squirrel cage induction motors and in part to the wide range of speed and torque output available. An application of the variable speed induction motor is in a sewage pumping station. The sewage pumping station, consisting of a well and pump, is required to maintain suitable output flow in the face of significant variations in input flow, on the order of seven to one [2]. Variable speed pumping using a d.c.-link converter, squirrel cage induction motor, and centrifugal pump is a potentially energy efficient method of maintaining output flows consistent with the variation in input flow [3, 4]. One potential difficulty associated with converter drive systems is poor system stability under some loading conditions [1, 5]. One of the design objectives of a feedback control system is to maintain adequate system stability margins over the expected range of operating conditions and system parameter variations [6]. Various design and

analysis methods are available which can be used to obtain a suitable feedback control law for linear systems; fewer are available for application to non-linear systems, of which the sewage pumping station is an example. One suggested approach is to use a combination of open loop control, which has associated with it a nominal state trajectory, and a linear perturbation feedback control law to maintain suitable system stability and disturbance rejection characteristics [7]. The present research is centered about applying modern control theory techniques to the design of a perturbation feedback control law for an example system; specifically, a sewage pumping station.

Approach

The overall system structure is summarized in figure 1. In this figure, the d.c.-link frequency converter supplies variable voltage and frequency power to the a.c. machine which drives a centrifugal pump. A squirrel cage induction motor and d.c.-link frequency converter drive is selected because of the simplicity and reliability of the squirrel cage induction motor. The pump output flow is chosen such that an appropriate level of sewage in the well is maintained under control of the nominal operating point algoritam, which takes into account the long term variations in input flow. The perturbation control system generates small changes to the nominal commanded voltage and frequency to improve short term stability and disturbance rejection characteristics of the system. The control

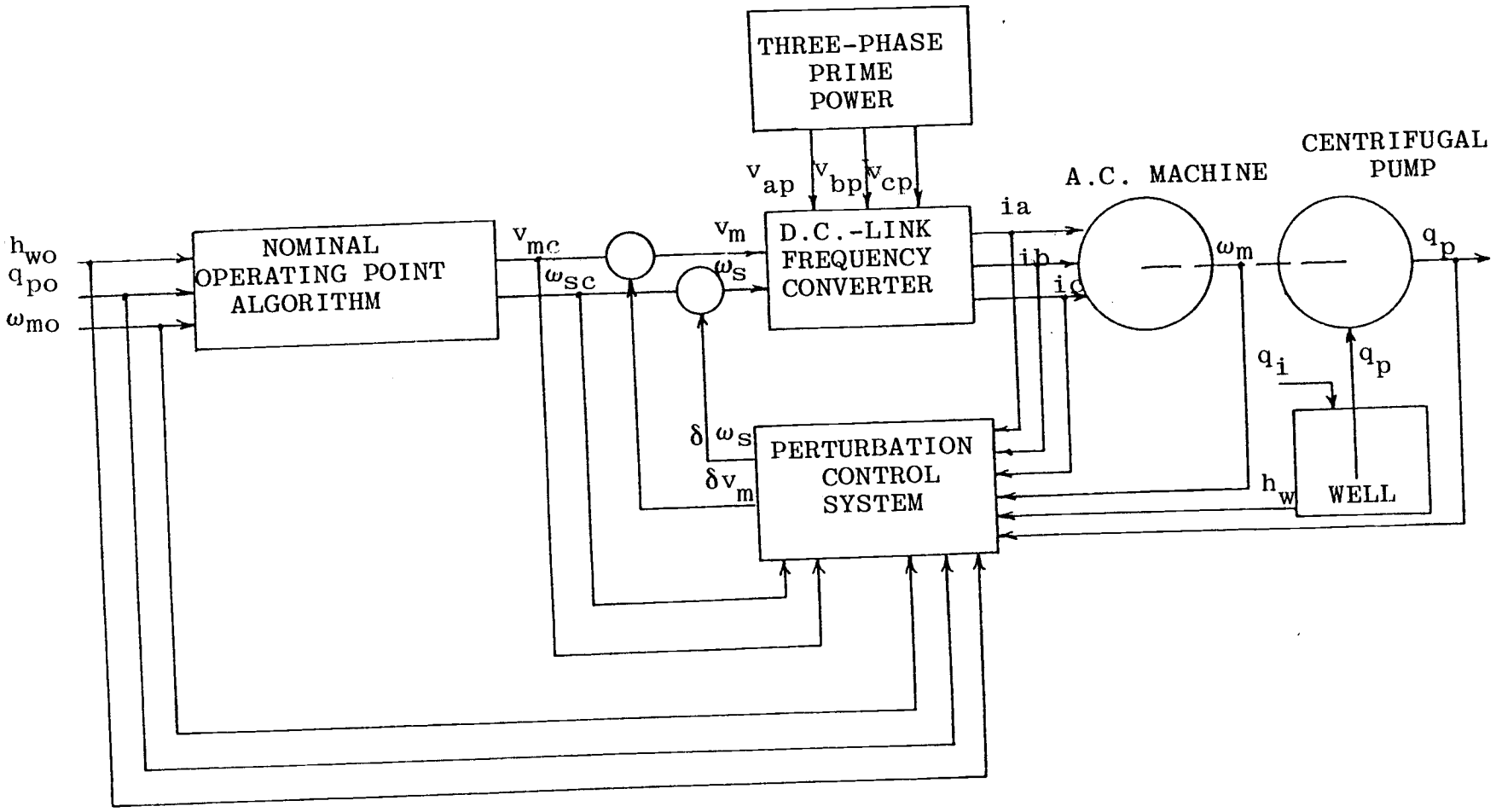

Figure 1. System Functional Schematic Diagram.

inputs are the amplitude and frequency of the fundamental component of the voltage applied to the stator windings of the induction machine. System states are stator current, rotor current, shaft frequency, output flow and well head. Model development and testing, and control system design and evaluation are addressed in the following chapters. The model development and testing consists of obtaining a suitable system of differential equations to represent the behavior of the actuator and plant. The induction machine model equations are simulated and the response of the simulation to a measured sinusoidal voltage is compared with the response of a 15 HP wound rotor induction machine to the same voltage waveform. Results of the model development and testing are presented in Chapter II.

Control system design and evaluation, presented in Chapter III, consists of evaluation of the linearized system model which forms the basis for the determination of the feedback control law using the steady state solution to the Ricatti equation associated with linear quadratic optimal control; evaluation of the resulting control system using a degital simulation of the overall system; and determination of the roots of the open loop and closed loop system characteristic equation at selected points along the simulated state trajectory. In Chapter IV, a summary of the results, conclusions, and recommendations for further research on this topic are presented.

Appendix A contains results of laboratory testing and analysis required to obtain estimates of the wound rotor induction machine parameters for use in the simulation response test, and appendix B presents a description, flow chart and list of inputs and outpus of the program used in the system simulation.

Summary

Linear optimal control system results are applied to the design of a perturbation control system for an example nonlinear system consisting of a d.c.-link frequency converter power supply, a squirrel cage induction machine, and a centrifugal pump associated with a sewage pumping station. A comparison of the response of the simulated induction machine and the response of a laboratory machine to a sinusoidal excitation is presented. Models of the elements of the system are combined to form an overall system model which, with the control system, is evaluated using a digital simulation. The perturbation control system pole placement is evaluated using transform methods.

II. MODEL DEVELOPMENT AND TESTING

Introduction

The sewage pumping station consists of a wet well into which sewage flows and a pumping system which maintains an appropriate level in the well in addition to control, monitoring and maintenance facilities. Certain constraints are imposed by the nature of the fluid, specifically (1) that the well not overlow, (2) that the contents of the well be changed such that septicity is avoided, and (3) flow in the main riser be maintained above a self-cleaning velocity [2]. In addition, it is desirable to minimize the energy required to operate the station. A mechanism which aids in achieving this goal is a variable speed pump [3]; hence, the system configuration includes a variable speed induction motor and centrifugal pump.

The subsystem models described in the following paragraphs are the induction motor, variable frequency power supply, and pump and hydraulic system. Additionally, results of a model verification test performed using a 15 HP wound rotor induction machine are described.

Induction Motor

The pump motor selected is a squirrel cage induction machine with a d.c.-link frequency converter power supply [1]. The model of the induction motor used is one based

on the symmetrical induction machine and developed by Robertson and Hebbar [8].

The symmetrical induction machine embodies the following assumptions: (1) uniform air gap, (2) linear magnetic circuit, (3) identical stator windings resulting in a sinusoidal mmf wave for balanced sinusoidal supply voltage, and (4) rotor bars such that the rotor mmf wave is sinusoidal with the same number of poles as the stator. While a number of possible terminal connections were considered in [8], only one terminal connection is considered here; specifically, no neutral connection and voltages applied to all three phases. Under these conditions, the following system of equations is obtained:

$$\underline{v} = R\underline{i} + L\frac{d}{dt}\underline{i}$$

where $\underline{v} = \begin{bmatrix} v_\alpha \\ v_\gamma \\ 0 \\ 0 \end{bmatrix}$

$$\underline{i} = \begin{bmatrix} i_{\alpha s} \\ i_{\gamma s} \\ i_{\alpha r} \\ i_{\gamma r} \end{bmatrix}$$

$$R = \begin{bmatrix} 2r_s & r_s & 0 & 0 \\ r_s & 2r_s & 0 & 0 \\ 0 & \frac{-3\sqrt{3}}{2} l_m \omega_m n & 2r_r & r_r - \frac{3\sqrt{3}}{2} l_r \omega_m n \\ \frac{3\sqrt{3}}{2} l_m \omega_m n & & r_r + \frac{3\sqrt{3}}{2} l_r \omega_m n & 2r_r \end{bmatrix}$$

$$L = \begin{bmatrix} 3l_s & \frac{3}{2} l_s & 3l_m & \frac{3}{2} l_m \\ \frac{3}{2} l_s & 3l_s & \frac{3}{2} l_m & 3l_m \\ 3l_m & \frac{3}{2} l_m & 3l_r & \frac{3}{2} l_r \\ \frac{3}{2} l_m & 3l_m & \frac{3}{2} l_r & 3l_r \end{bmatrix}$$

An additional equation which yields electromagnetic torque is given by

$$t_e = \frac{3\sqrt{3}}{2} l_m n (i_{\alpha s} i_{\gamma r} - i_{\gamma s} i_{\alpha r}).$$

The resulting motor differential equations are given by

$$\frac{d}{dt} \underline{i} = L^{-1} R \underline{i} + L^{-1} \underline{v}$$

The coefficients are given by

$$L^{-1}R = \frac{1}{d}\begin{bmatrix} \frac{3}{2}r_s l_r + \frac{cl_m^2 \omega_m n}{n} & cl_m^2 \omega_m n \\ -cl_m^2 \omega_m n & \frac{3}{2}l_s r_r - \frac{cl_m^2 \omega_m n}{2} \\ \frac{3}{2}l_m r_s - \frac{cl_m l_s \omega_m n}{2} & -cl_m l_s \omega_m n \\ cl_m l_s \omega_m n & \frac{3}{2}l_m r_s + cl_m l_s \omega_m n \end{bmatrix}$$

$$\begin{bmatrix} -\frac{3}{2}r_r l_m + \frac{cl_m l_r \omega_m n}{2} & cl_m l_r \omega_m n \\ -cl_m l_r \omega_m n & -\frac{3}{2}l_m l_r - \frac{cl_m l_r \omega_m n}{2} \\ \frac{3}{2}r_r l_s - \frac{cl_s l_r \omega_m n}{2} & -cl_s l_r \omega_m n \\ cl_s l_r \omega_m n & \frac{3}{2}r_r l_s + cl_s l_r \omega_m n \end{bmatrix}$$

where $c = \frac{3\sqrt{3}}{2}$

$d = \frac{3}{2}(l_s l_r - l_m^2)$

and

$$L^{-1} = \frac{1}{d}\begin{bmatrix} l_r & -\frac{l_r}{2} & -l_m & \frac{l_m}{2} \\ -\frac{l_r}{2} & l_r & \frac{l_m}{2} & -l_m \\ -l_m & \frac{l_m}{2} & l_s & -\frac{l_s}{2} \\ \frac{l_m}{2} & -l_m & -\frac{l_s}{2} & l_s \end{bmatrix}$$

For balanced sinusoidal supply voltages, the following transformation is attained between phase voltages and $\alpha-\gamma$ voltages

$$v_a = v_m \cos\theta$$

$$v_b = v_m \cos(\theta - 120)$$

$$v_c = v_m \cos(\theta + 120)$$

$$\underline{v} = \begin{bmatrix} v_\alpha \\ v_\gamma \\ 0 \\ 0 \end{bmatrix} = \begin{bmatrix} v_a - v_b \\ v_c - v_b \\ 0 \\ 0 \end{bmatrix}$$

$$v_\alpha = v_m (1.5 \cos\omega_s t - 0.866 \sin\omega_s t)$$

$$v_\gamma = v_m 1.732 \sin\omega_s t$$

Power Supply

The power supply, while based upon a d.c.-link converter [1], modeled as an idealized six-step waveform with negligible voltage and fundamental frequency switching times. If v_m and $_s$ are the amplitude and frequency of the fundamental component of the desired line to neutral voltage waveform, then the voltage amplitude and switching time are given by

$$v_d = \frac{\pi}{3} v_m,$$

$$t_s = \frac{\pi}{3} \frac{1}{\omega_s}.$$

Neglecting source impedance, the waveforms shown in Figure 2 are obtained using simple logic.

Pump and Hydraulics

A simplified representation of the pump and hydraulic system dynamics is given by the following equation [9].

$$t_p = k_t \omega_m^2$$

$$h_p = k_h \omega_m^2$$

$$h_f = k_f q_p^2 .$$

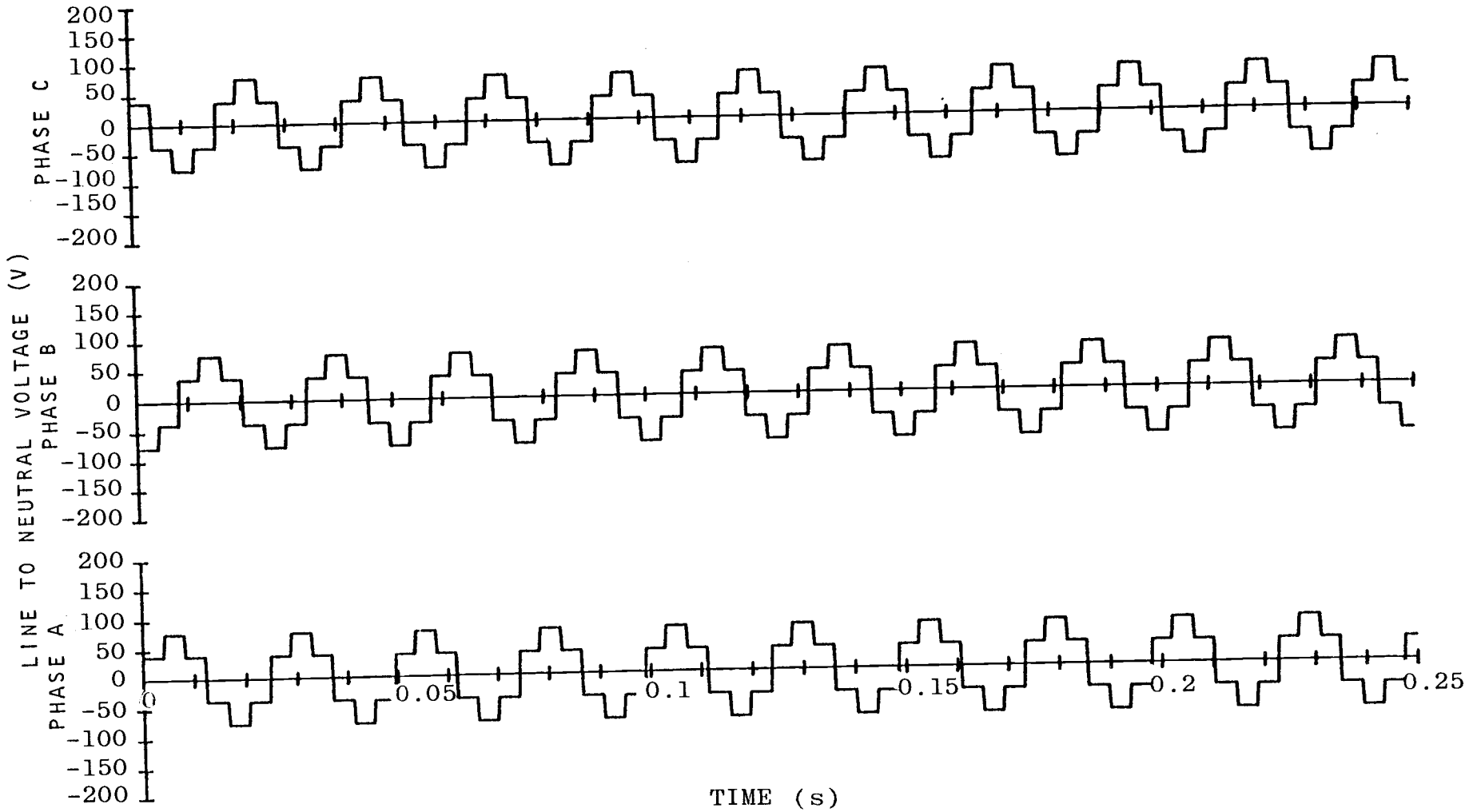

Figure 2. Idealized Power Supply Waveform.

The system output flow is given by

$$\frac{dq_p}{dt} = \frac{1}{m} \quad (h_p - h_s - h_f)$$

The well head is given by

$$\frac{dh_w}{dt} = k_w(q_i - q_p)$$

The values of the constants depend on the pump, pipe, and well characteristics. A specific example is presented in Chapter III.

Induction Motor Model Verification Test

Parameters for a Westinghouse wound rotor motor were determined experimentally and used in a simulation of the model equations previously presented. An experiment was conducted in which the induction motor was started; phase voltages, phase currents, and rotor speed were measured and recorded on an F.M. tape recorder during the starting transient. These data were digitized and the phase voltages were used as inputs to the simulation. The digitization process was accomplished using the Electrical and Computer Engineering hybrid computation laboratory to generate a magnetic tape containing the quantized values of the measured variables. The magnetic tape was then used to provide input to the computer program used in the simulation of the induction motor implemented on the Oregon State University com-

puter center Cyber-73 digital computer. The simulated response to measured phase voltages was calculated. The measured phase voltages are shown in Figure 3. A comparison of the measured and simulated phase current is shown for phase A, B, and C in Figures 4, 5, and 6, respectively. Figure 7 illustrates the agreement between measured and simulated rotor frequency. In these figures the error is given as the measured values subtracted from the simulated valves. Figure 8 is a plot of the simulated electromagnetic torque output of the motor. These figures illustrate the first 0.25 seconds of the starting transient.

Summary

A simplified model of a sewage pumping station consisting of a d.c.-link frequency converter, squirrel cage induction machine, and centrifugal pump and well has been developed and forms the basis for the design and evaluation of a perturbation feedback control law. An experiment was conducted to obtain a comparison between the induction machine model response and a 15 HP wound rotor machine to a senusoidal excitation. Comparison of simulated and measured currents, shown in Figures 4 through 6 indicate that the actual machine current amplitudes are significantly greater during starting than the simulated quantities. The maximum error during the starting transient occurs at 0.01 s in the phase A current as shown in Figure 4. The error amplitude at this point is approximately 125 A or 36% of

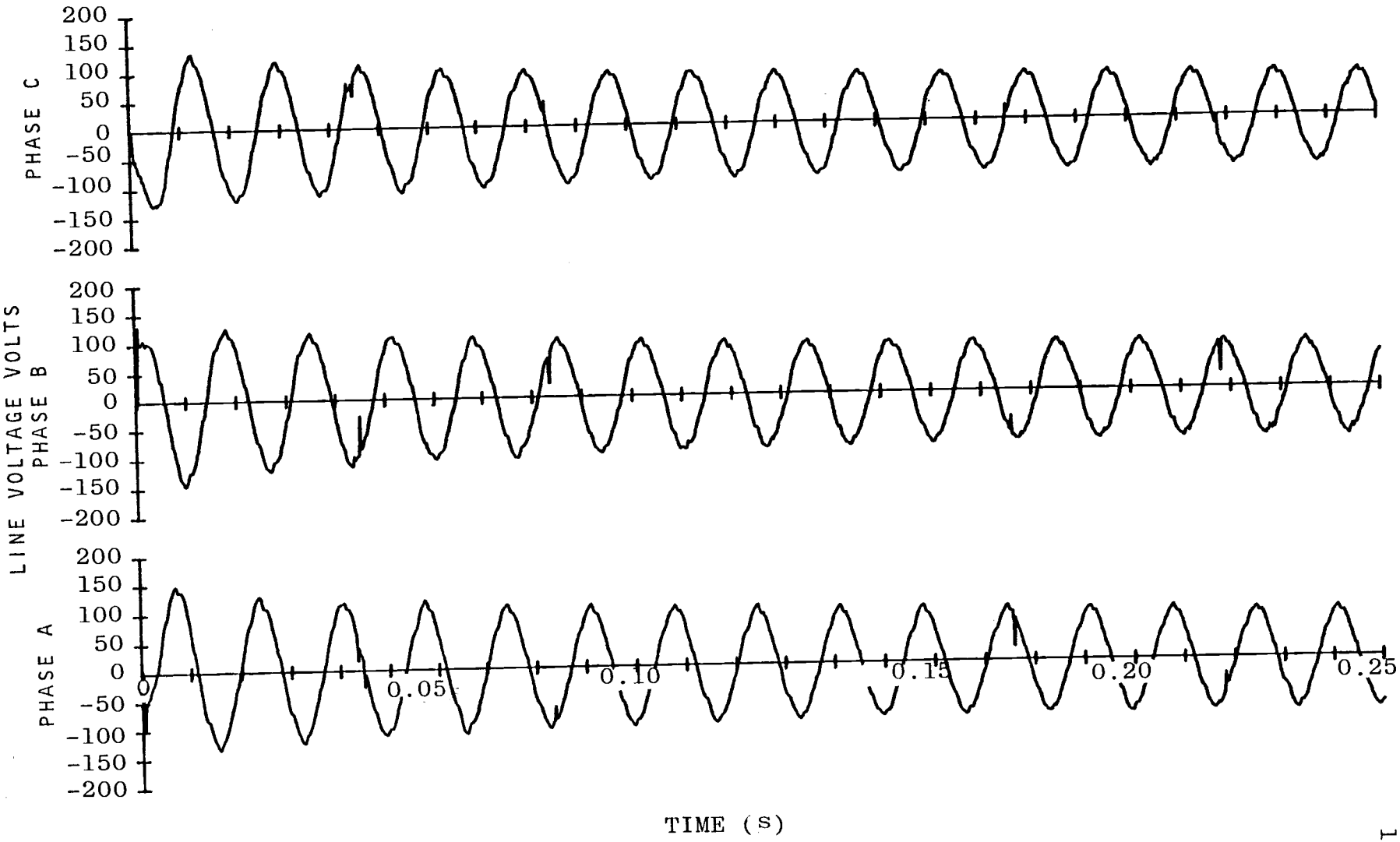

Figure 3. Measured Line-to-Neutral Voltages.

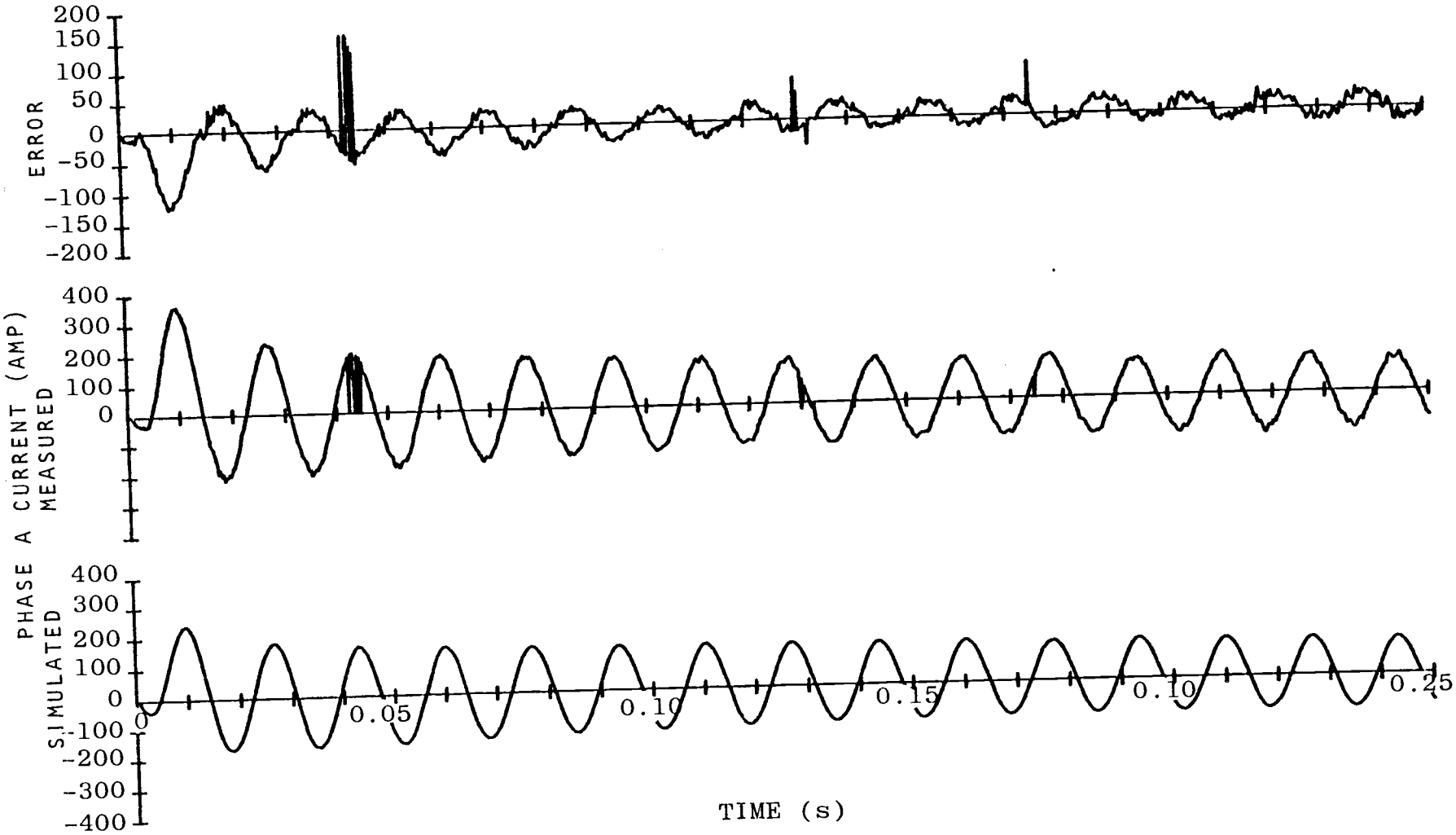

Figure 4. Comparison of Simulated and Measured Phase A Current.

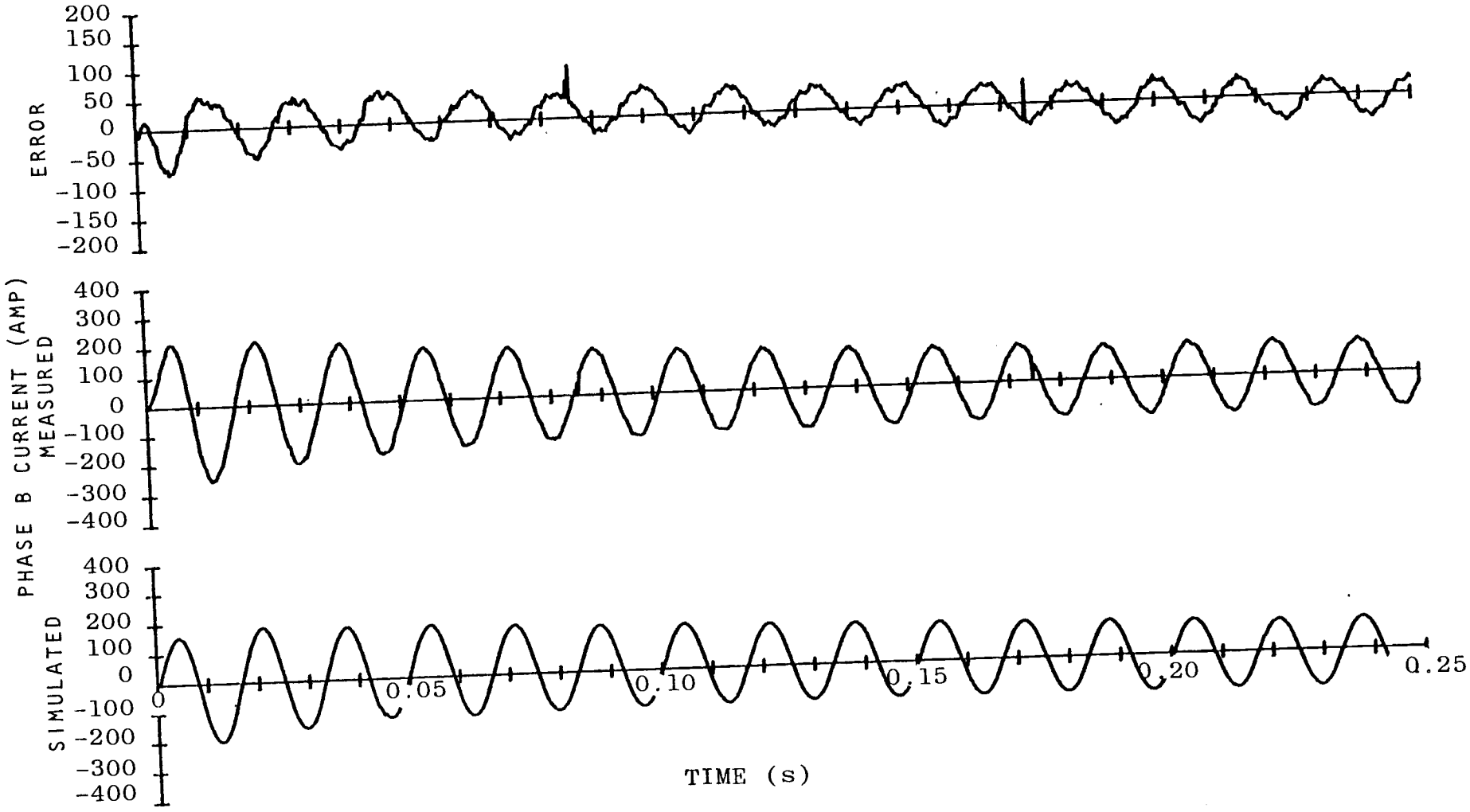

Figure 5. Comparison of Simulated and Measured Phase B Current.

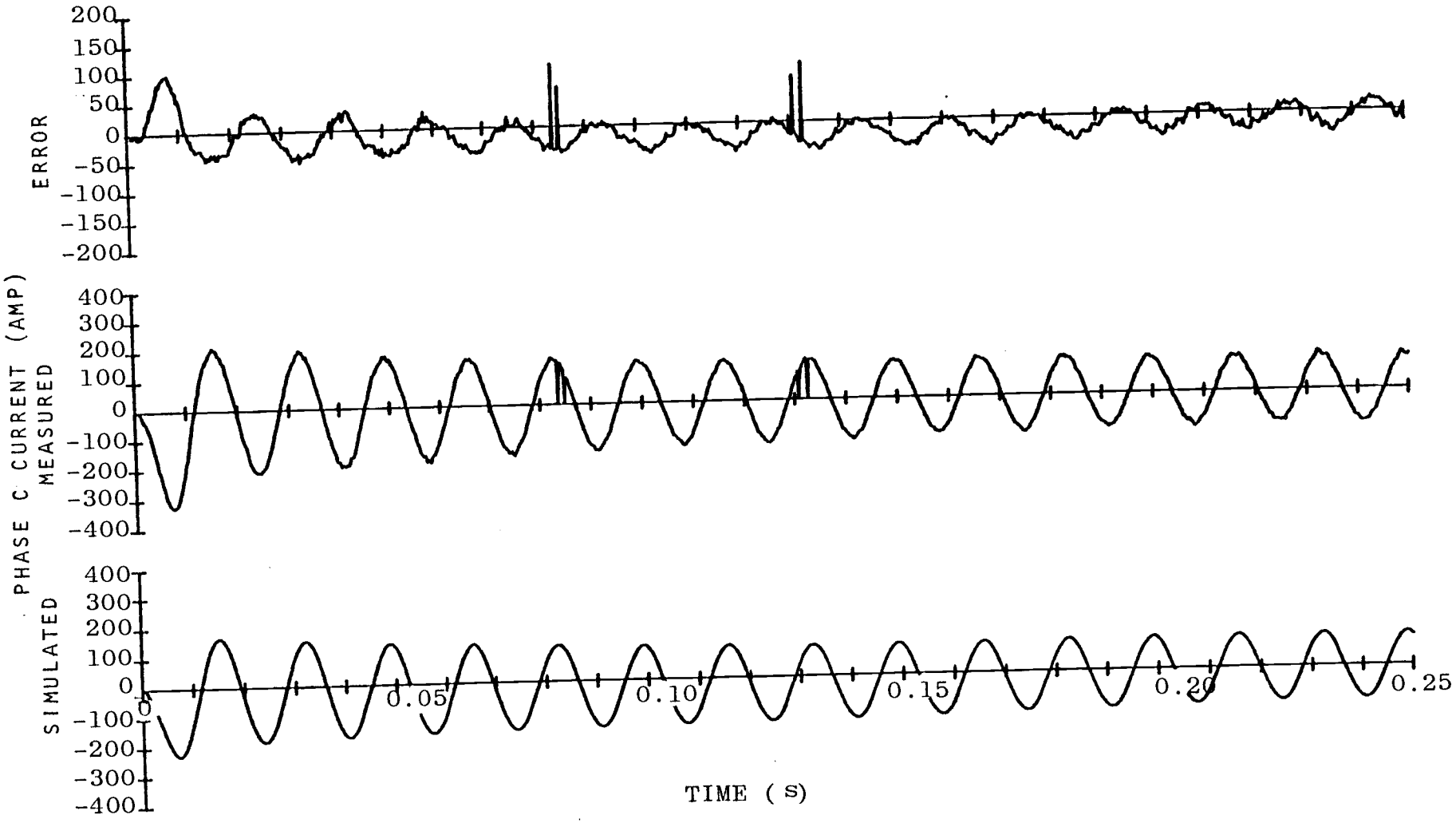

Figure 6. Comparison of Simulated and Measured Phase C Current.

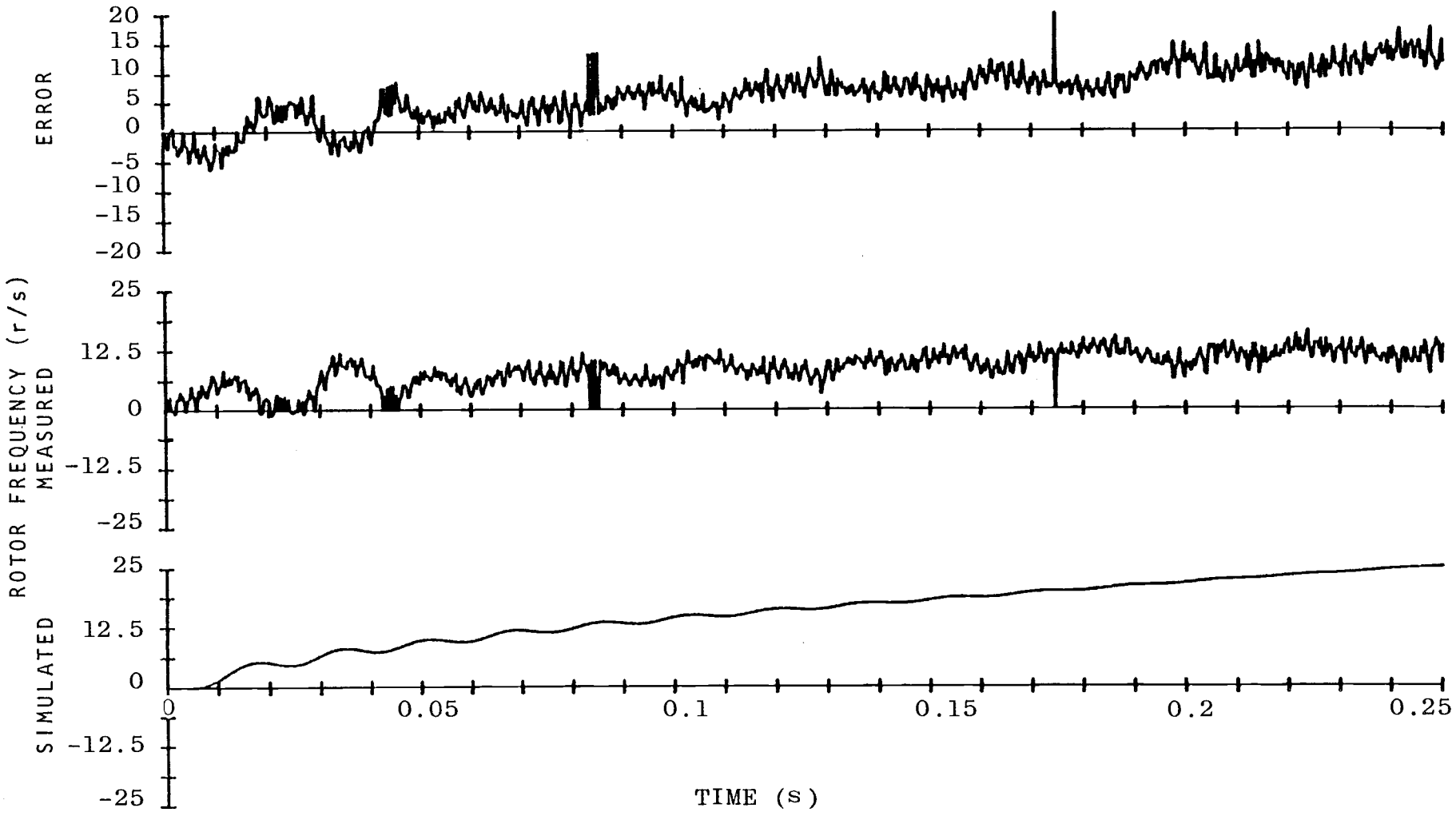

Figure 7. Comparison of Simulated and Measured Rotor Frequency.

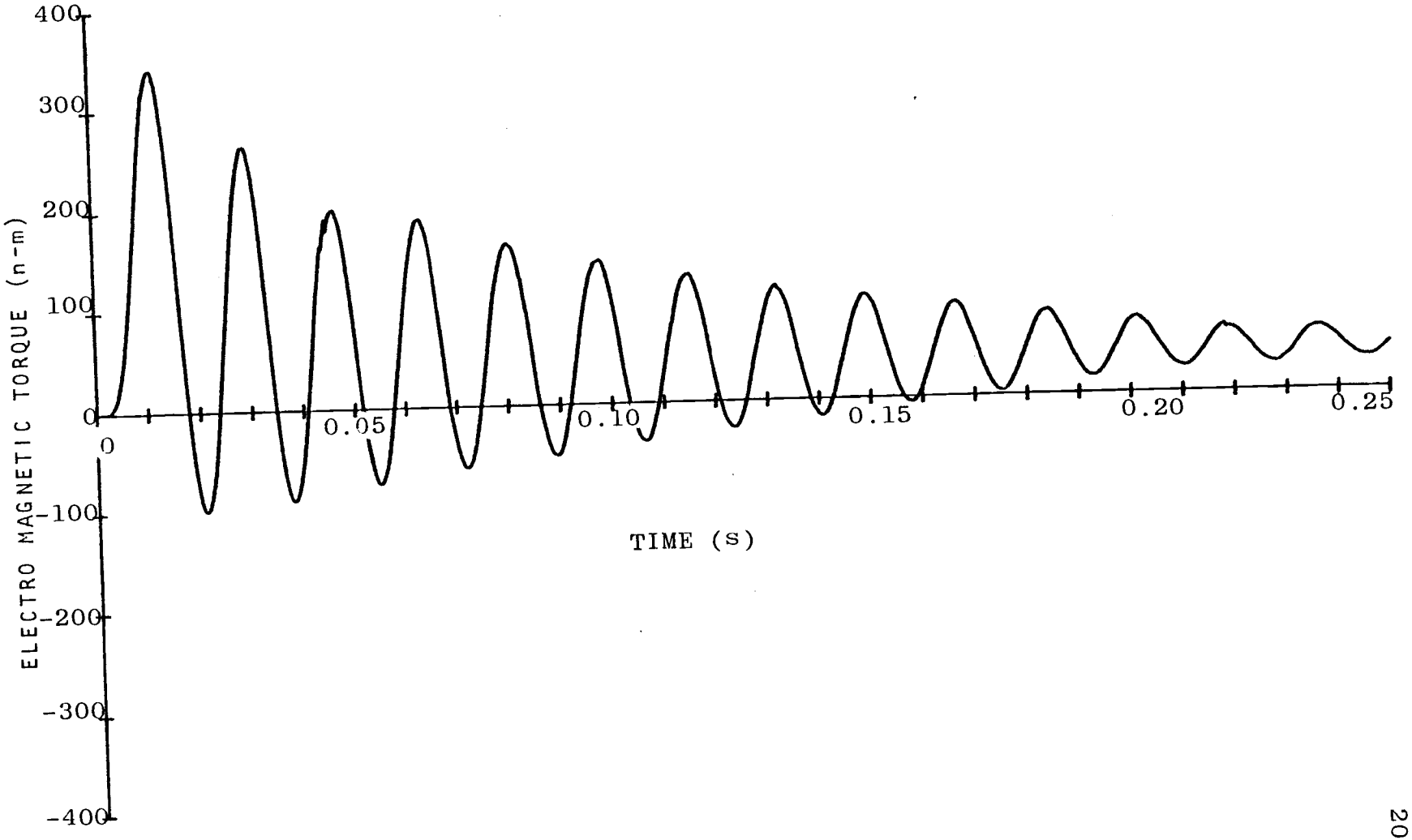

Figure 8. Simulated Electromagnetic Torque.

the measured line current. At 0.2 s the error is approximately 20 A or 20% of the measured line current. A potential cause for part of this error is evidenced in Figure 7. As can be seen from this figure, the simulated rotor frequency increases more rapidly than the measured rotor frequency. A potential cause for this effect is that the estimated damping to inertia ratio of the mechanical load is too small. This would tend to alter the effect of the speed voltage terms in the model equations such that the exhibited error in the line currents would occur.

III. CONTROL SYSTEM

Introduction

The control system design approach is based on a linearized representation of the system dynamics about the present state. The gains are calculated using a least squares cost functional and numerically obtaining the steady state solution to the discrete Riccati equation. All states are assumed to be available and noise free, either from direct measurements or implicitly assuming the existence of a suitable estimation algorithm. The sample period is chosen as the switching time of the power supply; hence, the sample period varies with the fundamental component frequency of the voltage waveform. The control--voltage magnitude and frequency--is calculated recursively by adding the inremental control to the previously calculated values. The initial commanded voltage and frequency is based on the steady-state operating point of the system.

Evaluation of the resulting control system performance is accomplished using a simulation of the nonlinear system dynamics, the power supply, and the feedback controller. Additionally, transfer functions for selected input-output pairs are evaluated in the frequency domain to assess sensitivity of the perturbation control system stability to variation in loop gain and phase.

The following paragraphs present the control system design and evaluation, and a summary of the results.

Control System Design

The nonlinear system is characterized by the system head curve, the pump performance characteristics and the motor performance. Preliminary sizing of system components is typically achieved by determining the input flow characteristics, designing the hydraulic and pump system and matching a suitable motor to the resulting hydraulic system. In the present instance, an example system is contrived which illustrates the short period (on the order of a few seconds) dynamic behavior of the overall system. The long term or quasi-steady state operating point is assumed to be provided by varying the desired output flow and well head setpoints, either manually or using a suitable flow-head profile computed automatically. The objective then is to design a controller which causes the flow and well head to track the slowly varying demand associated with diurnal, seasonal and weather induced variations in input flow.

The system head characteristics assumed are shown in Figure 9. This corresponds to a system with zero static head and a friction head coefficient

$$k_f = 9000 \text{ m}/(\text{m}^3/\text{sec})^2.$$

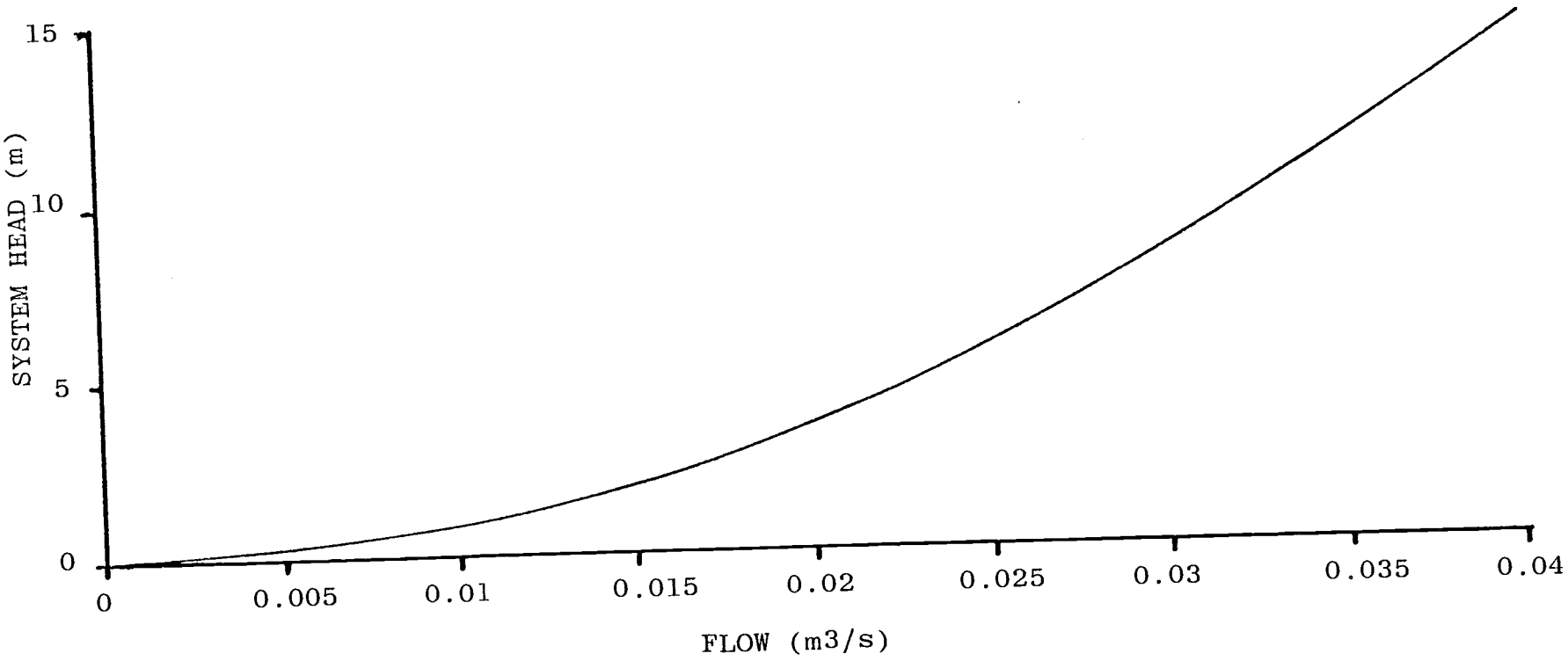

Figure 9. System Head Characteristics.

An idealized pump is assumed with the following characteristics:

reaction torque coefficient $k_t = 3.76 \times 10^{-3} \frac{\text{N-m}}{(\text{r/s})^2}$

output head coefficient $k_h = 8.21 \times 10^{-4} \frac{\text{m}}{(\text{r/s})^2}$

The pump characteristics are shown in Figure 10. This figure illustrates the required input torque and resulting output head as a function of shaft frequency. (The pump coefficients are based on a curve fit to the performance curves for Pacific Pumping Co. impeller 1262.)

The motor selected is a three-phase six-pole squirrel cage induction machine with power output at 60 Hz and 220 v rms line-to-line of approximately 7.5 kw. The motor parameter values are those of Example 9-1 of [10]. Steady state torque as a function of shaft frequency is shown in Figure 11 for balanced sinusoidal input voltages of various amplitudes. Also shown in this figure is the input power factor. These data were obtained using the per phase steady state equivalent circuit found in [10].

The solution for the feedback gains is based on a linearized representation of the system dynamics evaluated at the present state and control. The system equation is given by

$$\dot{x} = F(x, u)$$

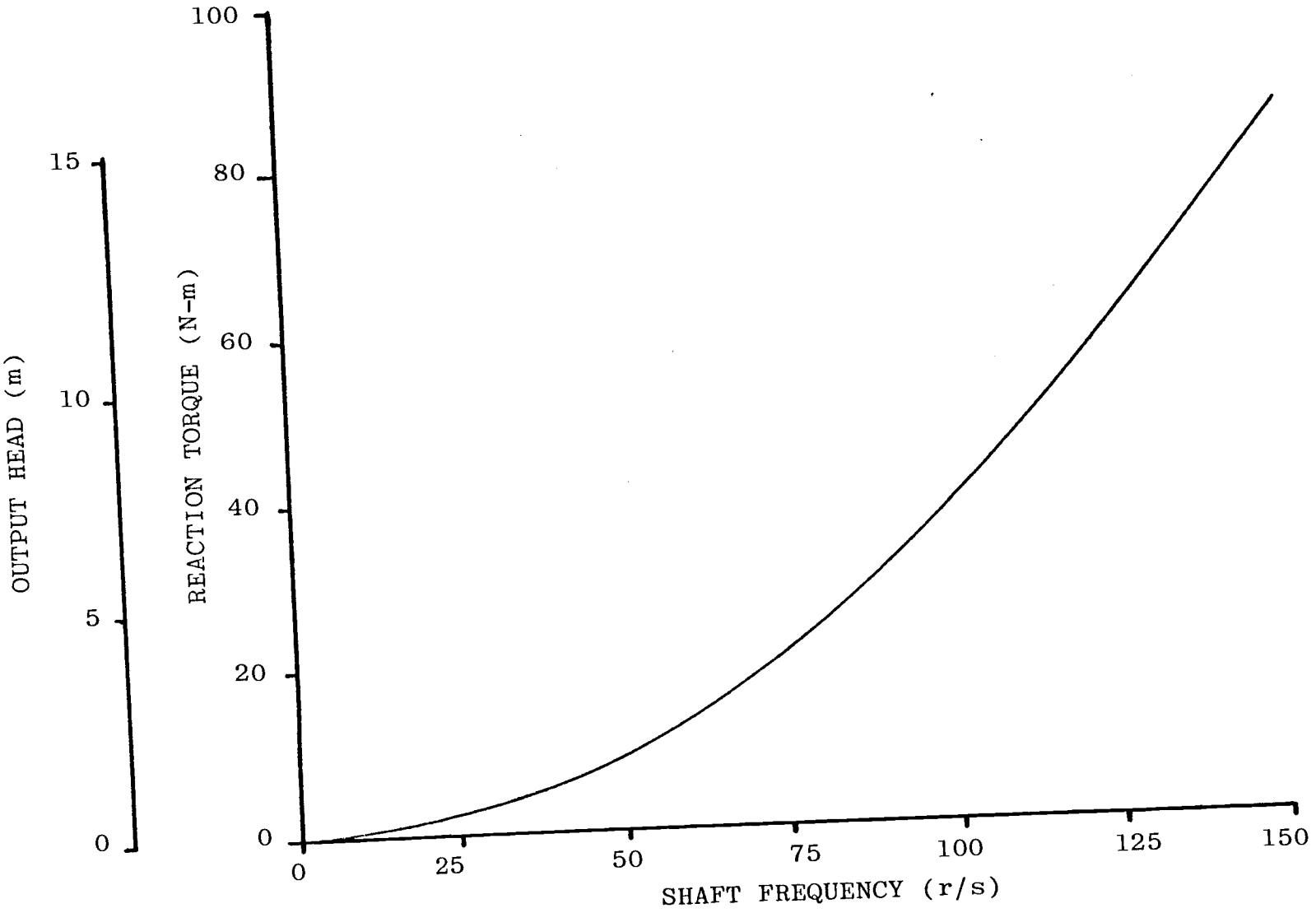

Figure 10. Pump Output Head and Reaction Torque Characteristics.

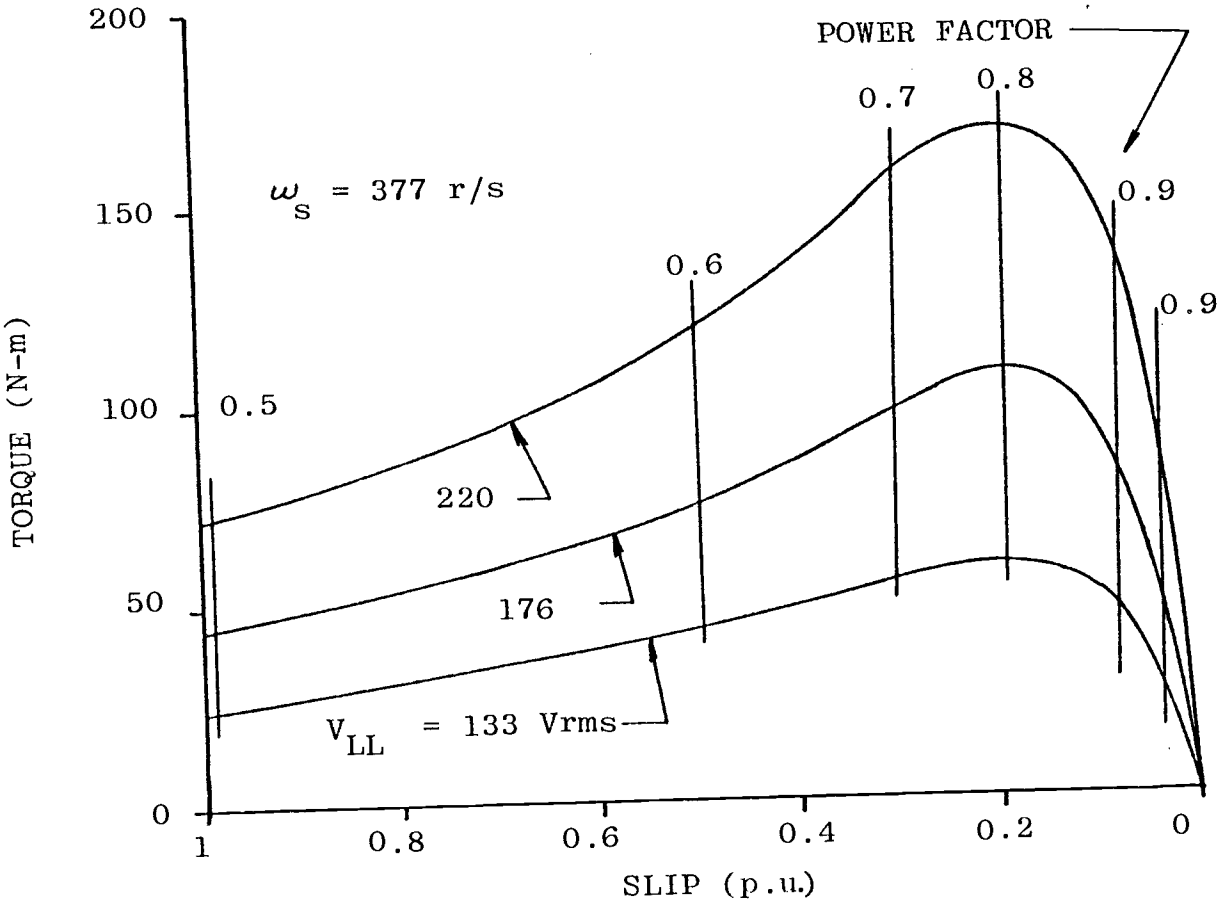

Figure 11. Induction Machine Torque-Speed Characteristics.

where

$$\underline{x} = \begin{bmatrix} i_{\alpha s} \\ i_{\gamma s} \\ i_{\alpha r} \\ i_{\gamma r} \\ \omega_m \\ q_p \\ h_w \end{bmatrix} \qquad \underline{u} = \begin{bmatrix} v_m \\ \\ \omega_s \end{bmatrix}$$

and F (x, u) is given by

$$\frac{d}{dt} i_{\alpha s} = \frac{1}{d}\left(\frac{3}{2} r_s l_r + \frac{c l_m^2 \omega_m n}{2}\right) i_{\alpha s} + \frac{c l_m^2 m^n}{d} i_{\gamma s} + \frac{1}{d}\left(-\frac{3}{2} r_r l_m + \frac{c l l_{mr} \omega_m n}{2}\right)$$

$$i_{\alpha r} + \frac{c l l_{mr} \omega_m n}{d} i_{\gamma r} + \frac{l_r}{d} v_\alpha \frac{-l_r}{2d} v_\gamma$$

$$\frac{d}{dt} i_{\gamma s} = \frac{1}{d} c l_m^2 \omega_m n i_{\alpha s} + \frac{1}{d}\left(\frac{3}{2} l_s r_r - \frac{c l_m^2 \omega_m n}{2}\right) i_{\gamma s} - \frac{1}{d} c l l_{mr} \omega_m n i_{\alpha r}$$

$$- \frac{1}{d}\left(\frac{3}{2} l_m r_r + \frac{c l_m l_r \omega_m n}{2}\right) i_{\gamma r} - \frac{l_r}{2d} v_\alpha + \frac{l_r}{d} v_\gamma$$

$$\frac{d}{dt} i_{\alpha r} = - \frac{1}{d}\left(\frac{3}{2} l_m r_s - \frac{c l_m l_s \omega_m n}{2}\right) i_{\alpha s} - \frac{1}{d} c l_m l_s \omega_m n i_{\gamma s} + \frac{1}{d}\left(\frac{3}{2} r_r l_s -\right.$$

$$\left. \frac{c l_s l_r \omega_m n}{2}\right) i_{\alpha r} - \frac{1}{d} c l_s l_r \omega_m n i_{\gamma r} - \frac{1}{d} v_\alpha + \frac{1}{2d} v_\gamma$$

$$\frac{d}{dt} i_{\gamma r} = \frac{1}{d} c l_m l_s \omega_m n i_{\alpha s} + \frac{1}{d}\left(-\frac{3}{2} l r_{ms} + \frac{c l l_{ms} \omega_m n}{2}\right) i_{\gamma s} + \frac{1}{d} c l_s l_r \omega_m n i_{\alpha r}$$

$$+ \frac{1}{d}\left(\frac{3}{2} r_r l_s + \frac{c l_s l_r \omega_m n}{2}\right) i_{\gamma r} + \frac{1}{2d} v_\alpha - \frac{1}{d} v_\gamma$$

$$\frac{d}{dt} \omega_m = \frac{1}{J} 2.6 l_m n \left(i_{\alpha s} i_{\gamma r} - i_{\gamma s} i_{\alpha r}\right) - \frac{D}{J} \omega_m - \frac{k_t}{J} \omega_m^2$$

$$\frac{d}{dt} q_p = \frac{k_h}{m} \omega_m^2 - \frac{h_s}{m} - \frac{k_f}{m} q_p^2$$

$$\frac{d}{dt} h_w = k_w \left(q_i - q_p\right)$$

Let $A = \frac{\partial F}{\partial x}(x_k, u_k)$,

$$B = \frac{\partial F}{\partial u}(x_k, u_k) \quad .$$

The elements of A and B are given by

$$a_{11} = \frac{1}{d}\left(\frac{3}{2} r_s l_r + \frac{cl_m^2 \omega_m n}{2}\right)$$

$$a_{12} = \frac{cl_m^2 \omega_m n}{d}$$

$$a_{13} = \frac{1}{d}\left(-\frac{3}{2} r_r l_m + \frac{cl\, l_{mr}\, \omega_m n}{2}\right)$$

$$a_{14} = \frac{cl_m l_r \omega_m n}{d}$$

$$a_{15} = \frac{cl_m^2 n}{2d} i_{\alpha s} + \frac{cl_m^2 n}{d} i_{\gamma s} + \frac{cl_m l_r n}{2d} i_{\alpha r} + \frac{cl_m l_r n}{d} i_{\gamma r}$$

$$a_{16} = 0$$

$$a_{17} = 0.$$

$$a_{21} = -\frac{cl_m^2 \omega_m n}{d}$$

$$a_{22} = \frac{1}{d}\left(\frac{3}{2} l_s r_r - \frac{cl_m^2 \omega_m n}{2}\right)$$

$$a_{23} = -\frac{1}{d} cl_m l_r \omega_m n$$

$$a_{24} = -\frac{1}{d}\left(\frac{3}{2} l_m r_r + \frac{cl_m l_r \omega_m n}{2}\right)$$

$$a_{25} = -\frac{1}{d} cl_m^2 n\, i_{\alpha s} - \frac{cl_m^2 n}{2d} i_{\gamma s} - \frac{-cl_m l_r n}{d} i_{\alpha r} - \frac{cl_m l_r n}{2d} i_{\gamma r}$$

$$a_{26} = 0.$$

$$a_{27} = 0.$$

$$a_{31} = -\frac{1}{d}\left(\frac{3}{2} l_m r_s - \frac{cl_m l_s \omega_m n}{2}\right)$$

$$a_{32} = -\frac{1}{d} cl_m l_s \omega_m n$$

$$a_{33} = \frac{1}{d}\left(\frac{3}{2} r_r l_s - \frac{cl_s l_r \omega_m n}{2}\right)$$

$$a_{34} = -\frac{cl_s l_r \omega_m n}{d}$$

$$a_{35} = \frac{cl_m l_s n}{2d} i_{\alpha s} - \frac{cl_m l_s n}{d} i_{\gamma s} - \frac{cl_s l_r n}{2d} i_{\alpha r} \frac{cl_s l_r n}{d} i_{\gamma r}$$

$$a_{36} = 0.$$

$$a_{37} = 0.$$

$$a_{41} = \frac{cl_m l_s \omega_m n}{d}$$

$$a_{42} = \frac{1}{d}\left(-\frac{3}{2} l_m r_s + \frac{cl_m l_s \omega_m n}{2}\right)$$

$$a_{43} = \frac{cl_s l_r \omega_m n}{d}$$

$$a_{44} = \frac{1}{d}\left(\frac{3}{2} r_r l_s + \frac{c l_s l_r \omega_m n}{2}\right)$$

$$a_{45} = \frac{c l_m l_s n i_{\alpha s}}{d} + \frac{c l_m l_s n\, i_{\gamma s}}{2d} + \frac{c l_s l_r n i_{\alpha r}}{d} + \frac{c l_s l_r n\, i_{\gamma r}}{2d}$$

$$a_{46} = 0.$$

$$a_{47} = 0.$$

$$a_{51} = \frac{2.6\, l_m n\, i_{\gamma r}}{J}$$

$$a_{52} = \frac{2.6\, l_m n\, i_{\alpha r}}{J}$$

$$a_{53} = \frac{2.6\, l_m n\, i_{\gamma s}}{J}$$

$$a_{54} = \frac{2.6\, l_m n\, i_{\alpha s}}{J}$$

$$a_{55} = -\frac{1}{J}\left(D + k_t \omega_m\right)$$

$$a_{56} = 0.$$

$$a_{57} = 0.$$

$$a_{61} = 0.$$

$$a_{62} = 0.$$

$$a_{63} = 0.$$

$$a_{64} = 0.$$

$$a_{65} = \frac{k_h \omega_m}{m}$$

$$a_{66} = -\frac{k_f q_p}{m}$$

$$a_{67} = 0.$$

$$a_{71} = 0.$$

$$a_{72} = 0.$$

$$a_{73} = 0.$$

$$a_{74} = 0.$$

$$a_{75} = 0.$$

$$a_{76} = k_w$$

$$a_{77} = 0.$$

$$b_{11} = \frac{l_r}{d} (1.5 \cos\theta)$$

$$b_{12} = -\frac{V\ T\ l_r}{d} 1.5 \sin\theta$$

$$b_{21} = -\frac{l_r}{d} (1.5 \cos\theta + 1.299 \sin\theta)$$

$$b_{22} = \frac{V\ T\ l_r}{d}\ (0.75 \sin\theta - 2.165 \cos\theta)$$

$$b_{31} = -\frac{l}{d}\ 1.5 \cos\theta$$

$$b_{32} = -\frac{V\ T\ l_m}{d}\ 1.5 \sin\theta$$

$$b_{41} = \frac{l}{d}\ (0.75 \cos\theta + 1.299 \sin\theta)$$

$$b_{42} = \frac{V\ T\ l_m}{d}\ (-0.75 \sin\theta + 2.165 \cos\theta)$$

where $\theta = \omega_s t$

The perturbation equation is given by

$$\underline{\delta\dot{x}} = A\ \underline{\delta x} + B\ \underline{\delta u}.$$

The feedback gains are given by the steady state solution to the discrete Ricatti equation. The sampling process is carried out in the following approximate form:

Let $\phi = e^{AT}$

$$\xi = \int_0^T e^{A\tau}\ d\tau$$

ϕ and ξ are given by the series approximation

$$\phi = I + AT + \frac{A^2T^2}{2!} + \ldots + \frac{A^{10}T^{10}}{10!} ,$$

$$\xi = TI + \frac{AT^2}{2!} + \ldots + \frac{A^{10}T^{11}}{11!} .$$

Let $\psi = \xi B$

then

$$\underline{x}_k = \phi \underline{x}_{k-1} + \psi \underline{u}_k$$

the equation for the feedback gains are, in recursive form [11].

$$G = - [\psi' W_k \psi + R]^{-1} \psi' W_k$$

$$W_{k+1} = \psi' W_k \psi G + \phi' W_k \phi + Q$$

where the cost functional is

$$I = \lim_{N \to \infty} \frac{1}{2} \sum_{i=k}^{N-1} (x' Qx + u'Ru)_i$$

and $Q \geq 0$, $R > 0$.

Steady state values are obtained at each sample time by iterating the gain equations until

$$\frac{trW_k - trW_{k+1}}{trW_k} < 0.1$$

or until 10 iterations occur.

The control system equations are given by

$$\underline{\delta u}_{k+1} = G_{k+1}\, \underline{\delta x}_k$$

$$\underline{u}_{k+1} = \underline{u}_k + \underline{\delta u}_{k+1} \quad .$$

where u is the amplitude of the line-to-neutral phase voltage and the frequency of the fundamental component of the voltage waveform.

Control System Evaluation

Evaluation of the control system is accomplished using a simulation of the overall system and by evaluating the frequency response of selected input-output pairs at various operating points.

Simulation

The system simulation is implemented for the digital computer using FORTRAN. (The program flow chart and list of inputs and outputs are in Appendix B.) The objective of the simulation is to evaluate system response during starting and to verify that the steady-state operating point is achieved as predicted. The simulation block diagram is shown in Figure 12 . The transient response during the first 0.25 seconds is shown in Figures 13 through 17 .

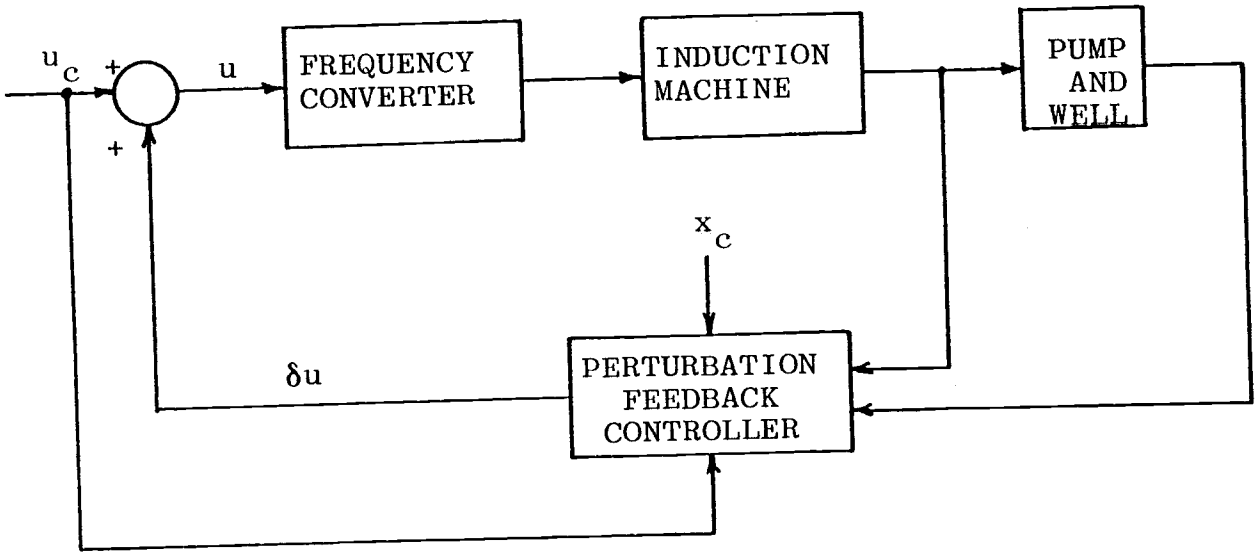

Figure 12. Simulation Block Diagram.

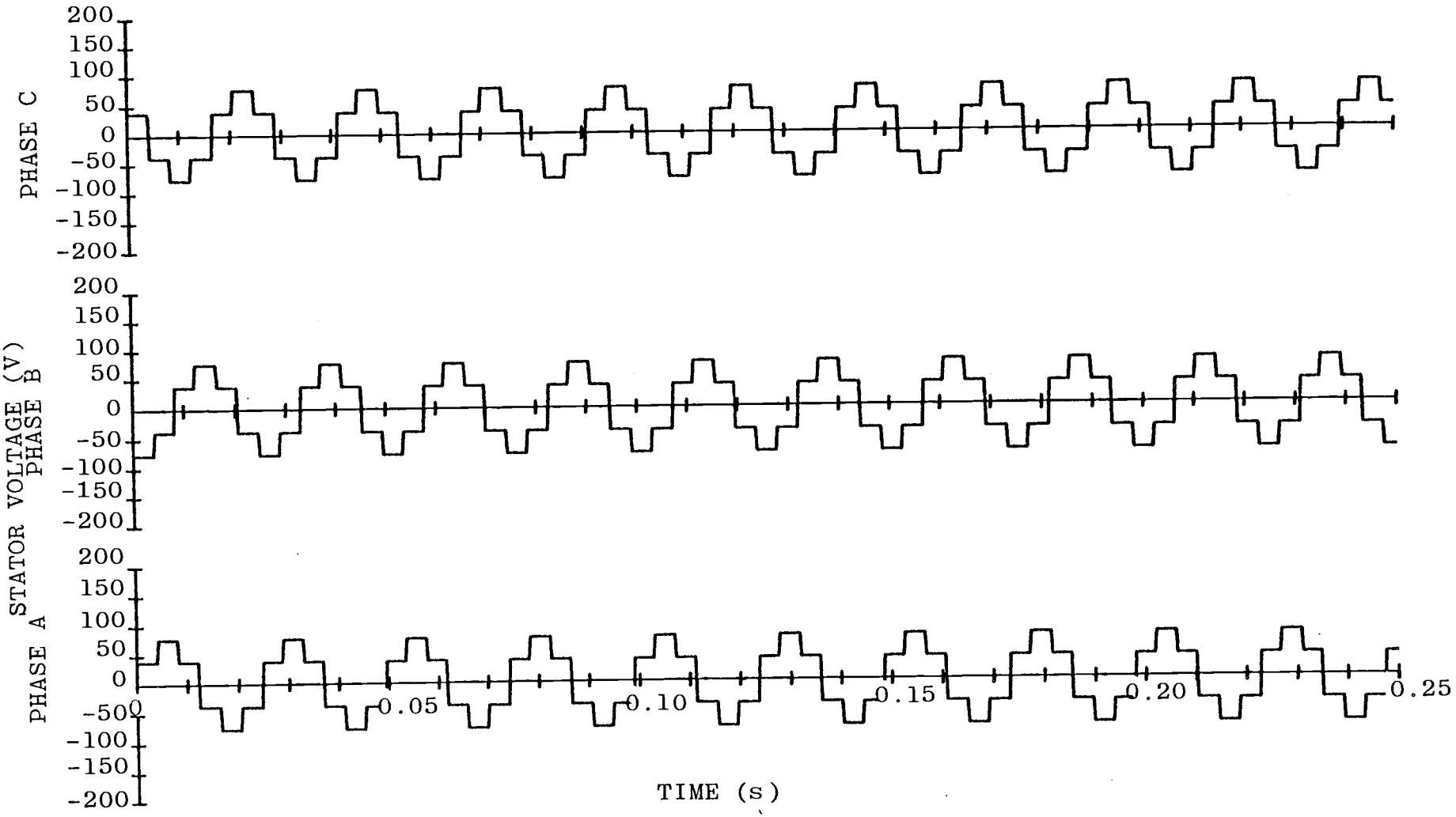

Figure 13. Stator Voltage During Open Loop Starting.

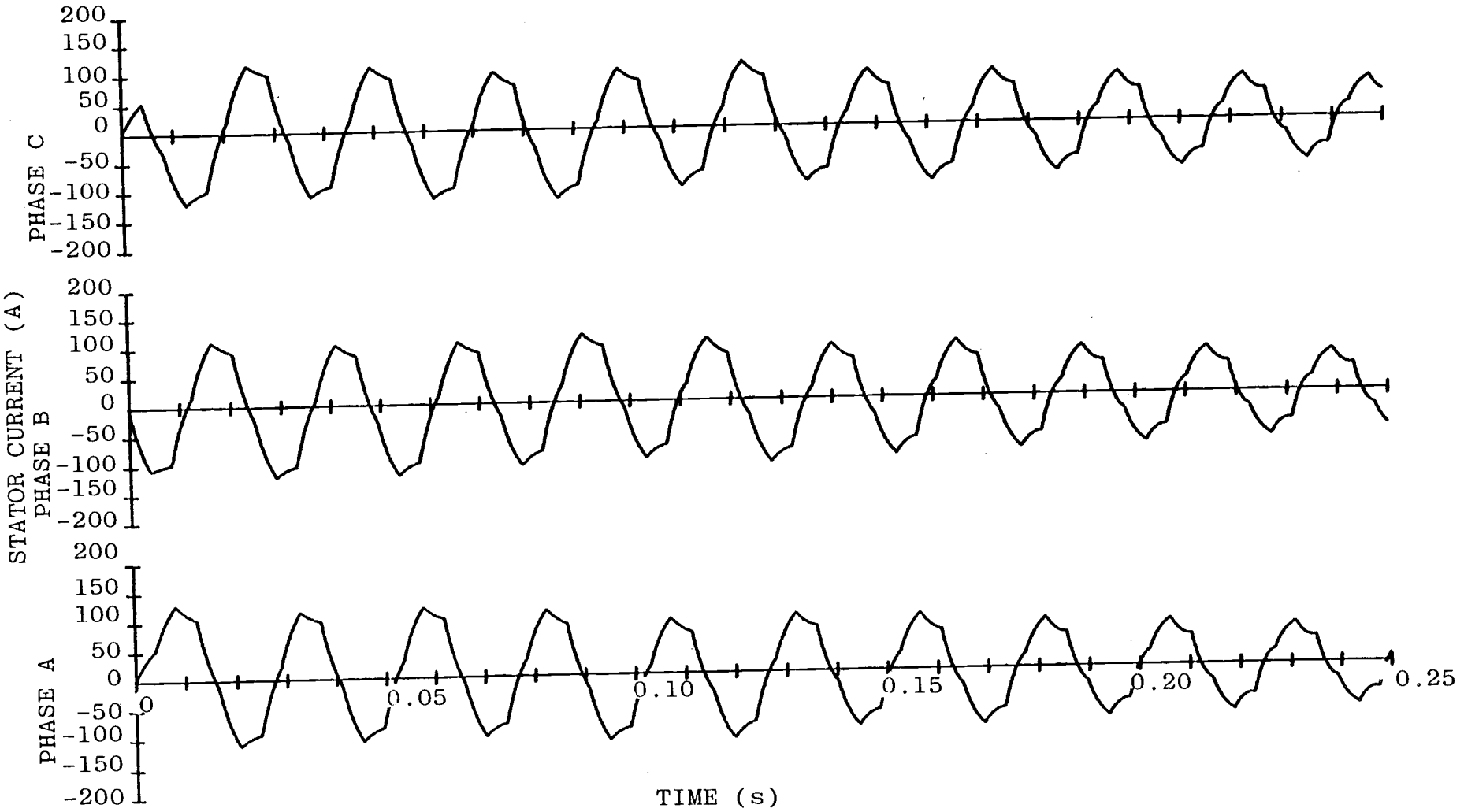

Figure 14. Stator Current During Open Loop Starting.

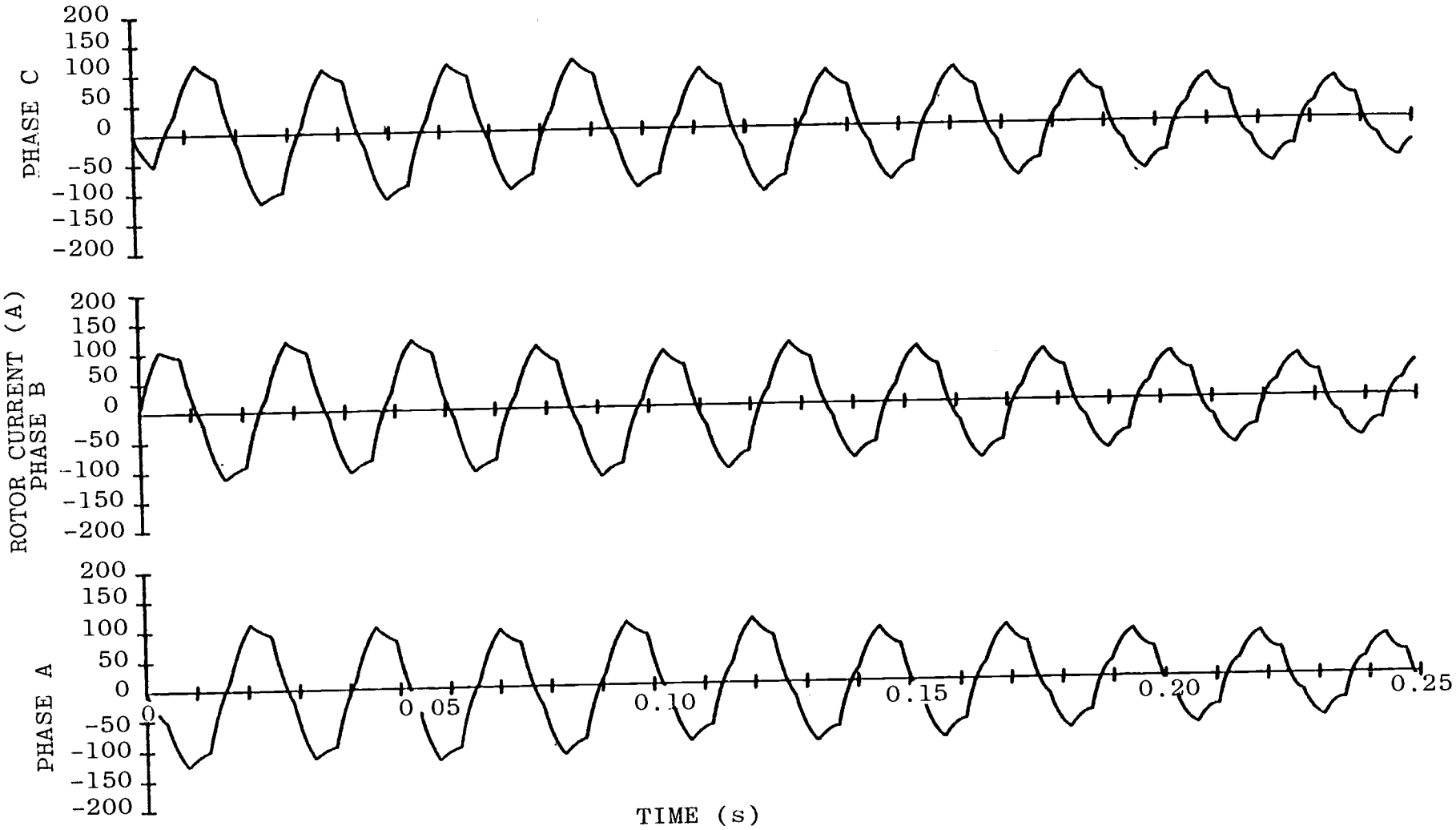

Figure 15. Rotor Current Referred to the Stator During Starting.

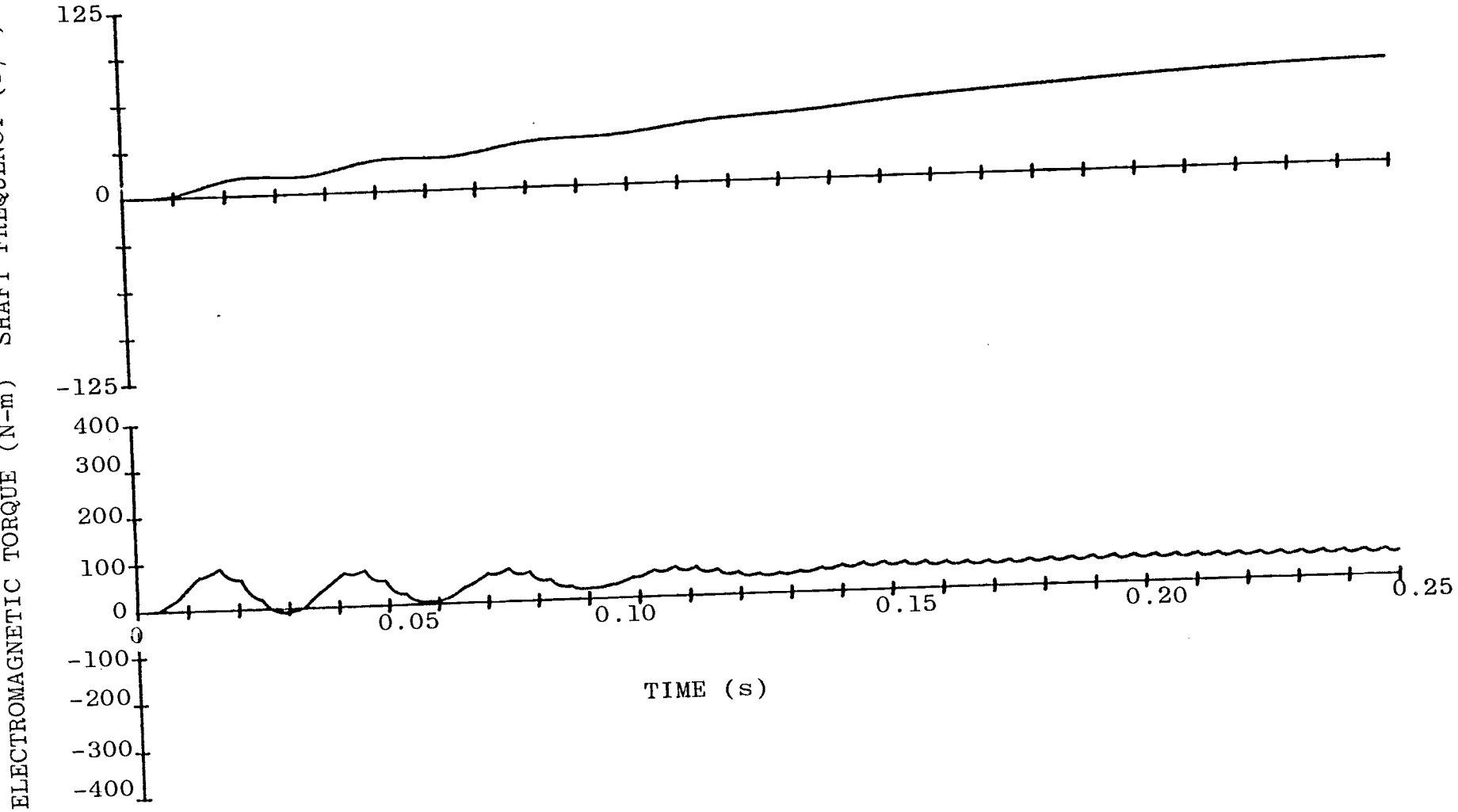

Figure 16. Electromagnetic Torque and Shaft Frequency During Open Loop Starting.

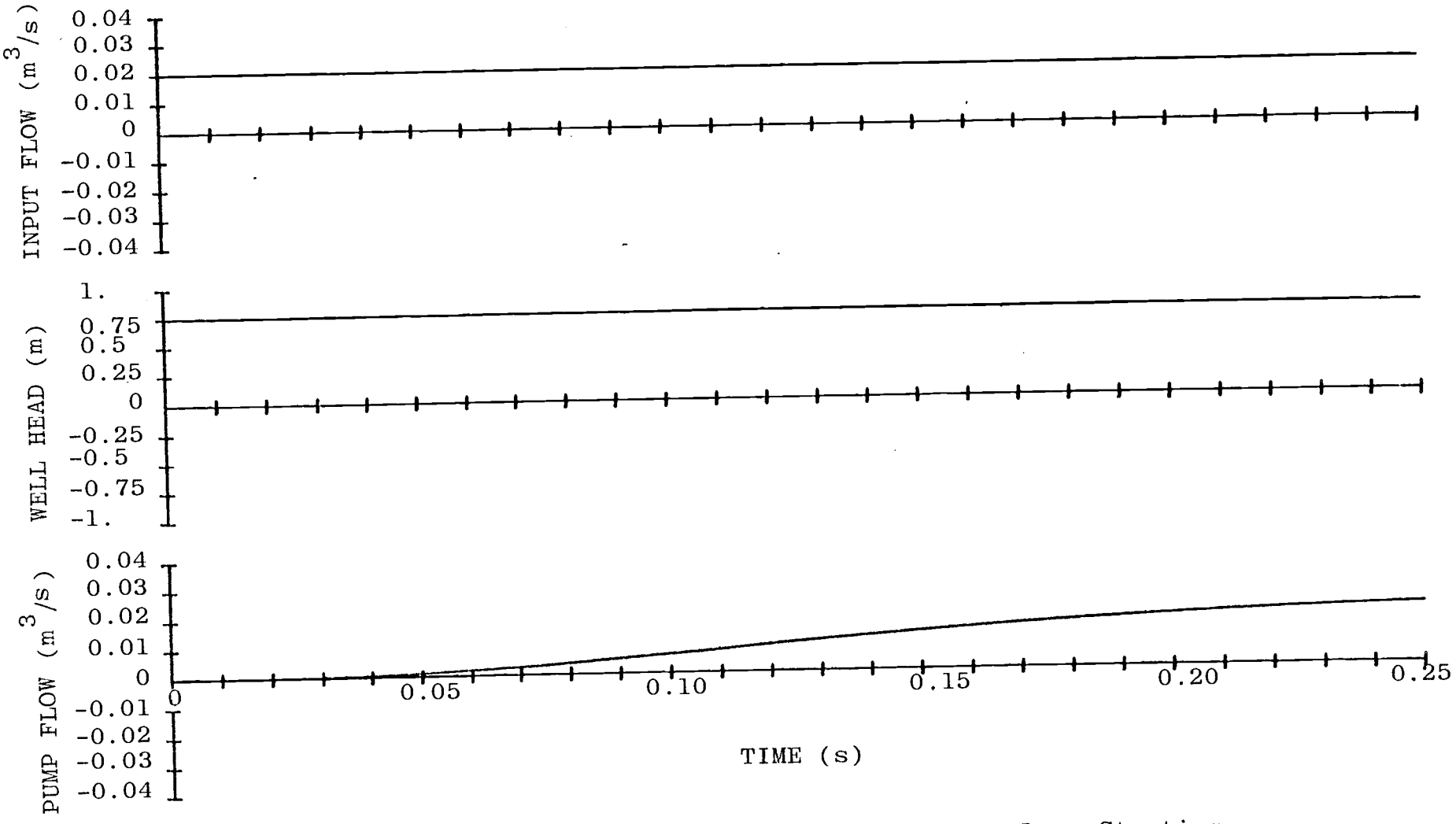

Figure 17. Pump Flow, Input Flow, and Well Head During Open Loop Starting.

At t = 0.5 s, the feedback control loop is closed. The weighting coefficients in the cost function are used in this case are

State Weighting

$$Q = \text{diag}\,(1 \times 10^{-6} \quad 1 \times 10^{-6} \quad 1 \times 10^{-6} \quad 1 \times 10^{-6}$$
$$7 \times 10^{-2} \quad 1.4 \times 10^{3} \quad 1.4 \times 10)$$

Control Weighting

$$R = \text{diag}\,(1.5 \times 10^{-5} \quad 3 \times 10^{-5}).$$

The nominal state is

$$x_c = (0 \quad 0 \quad 0 \quad 0 \quad 68. \quad 0.02 \quad 0.75)',$$

and the nominal control is

$$u = (110 \quad 255)'.$$

On the first cycle of closed loop control, the gain equations required five iterations to converge; subsequently, the gain equations converged on the first iteration. The system operation under closed loop control during 0.25 s starting at t = 0.75 s is shown in Figures 18 through 23.

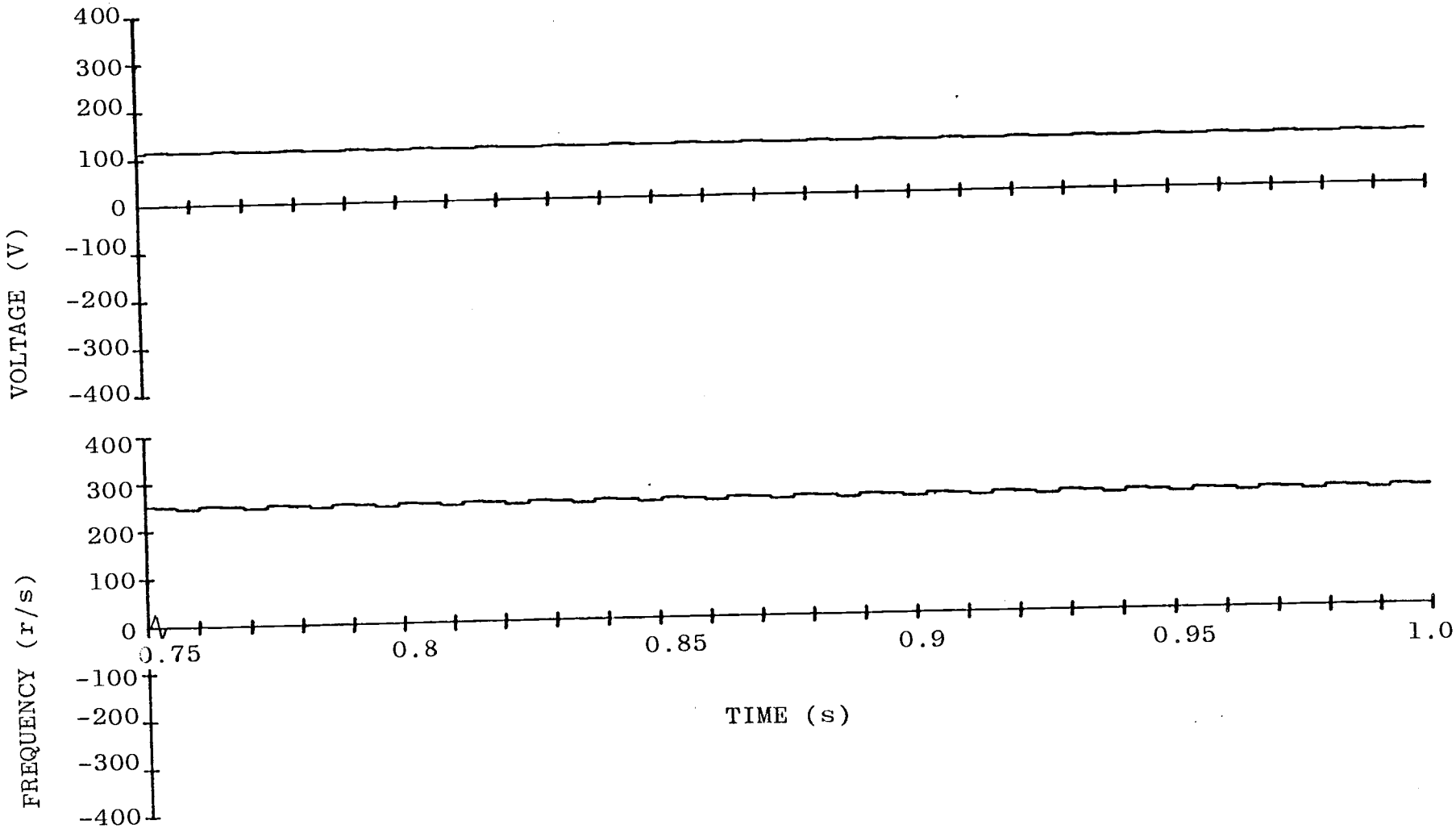

Figure 18. Commanded Voltage and Frequency During Closed Loop Operation.

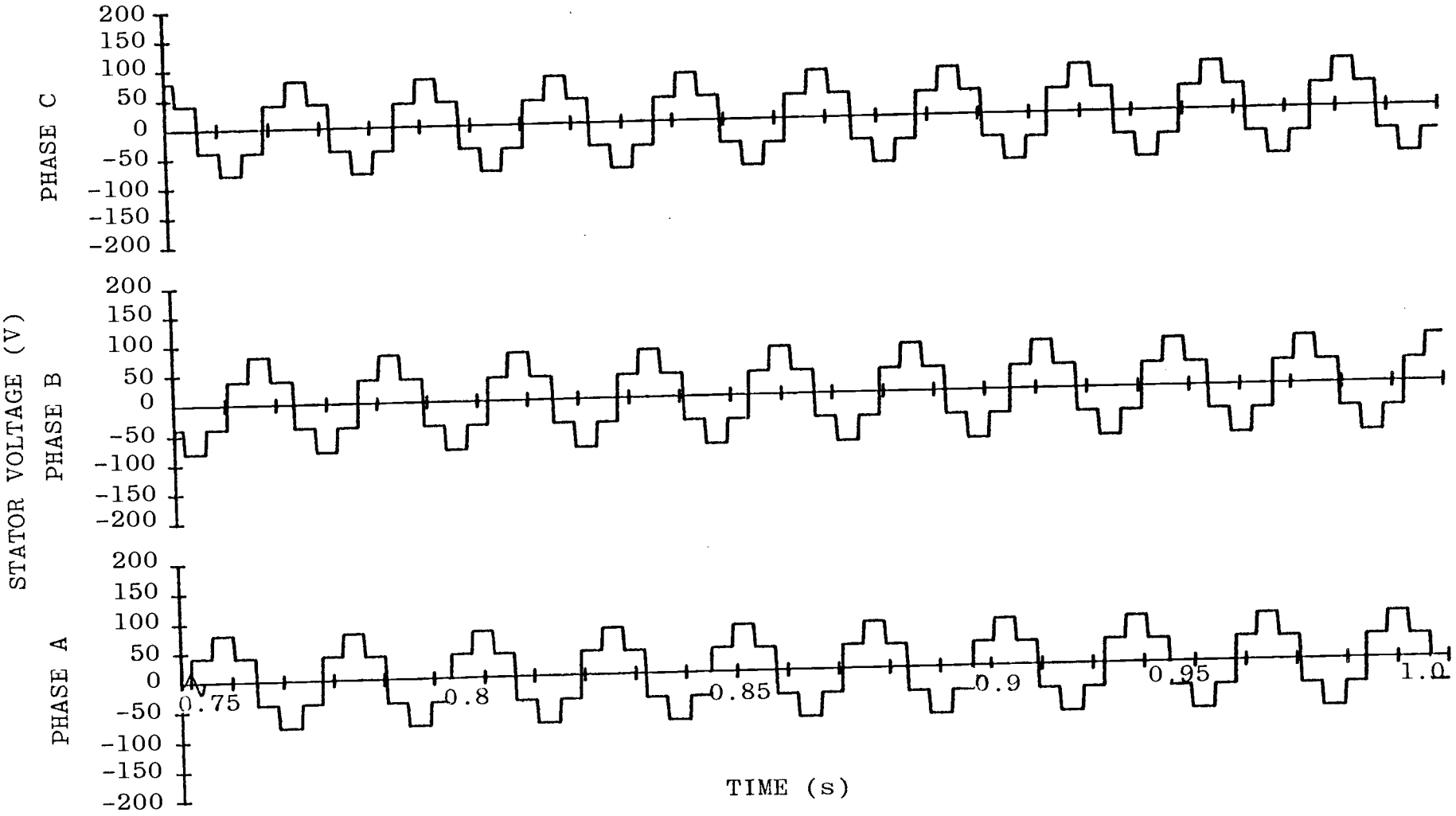

Figure 19. Power Supply Output Voltage During Closed Loop Operation.

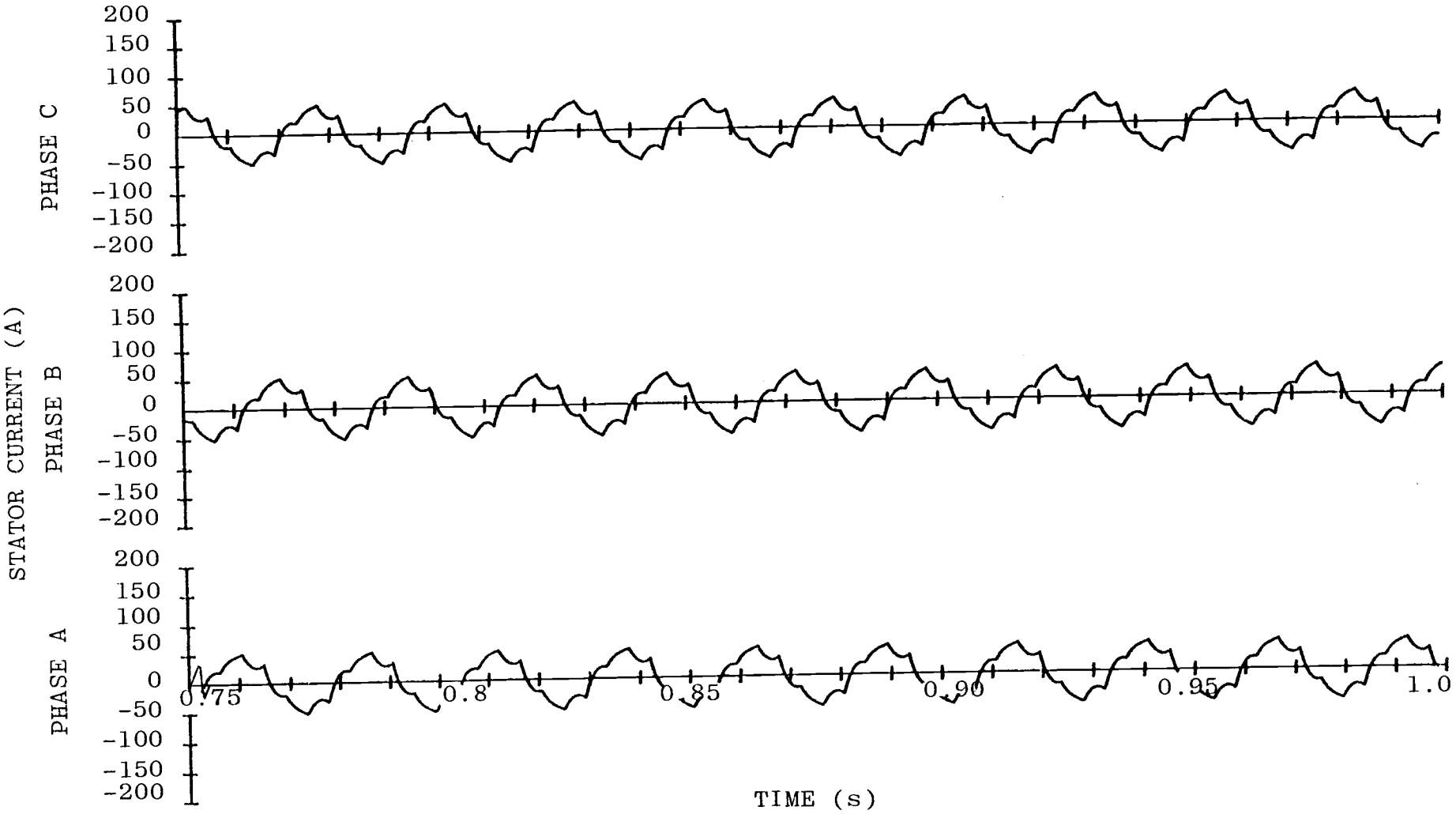

Figure 20. Stator Current During Closed Loop Operation.

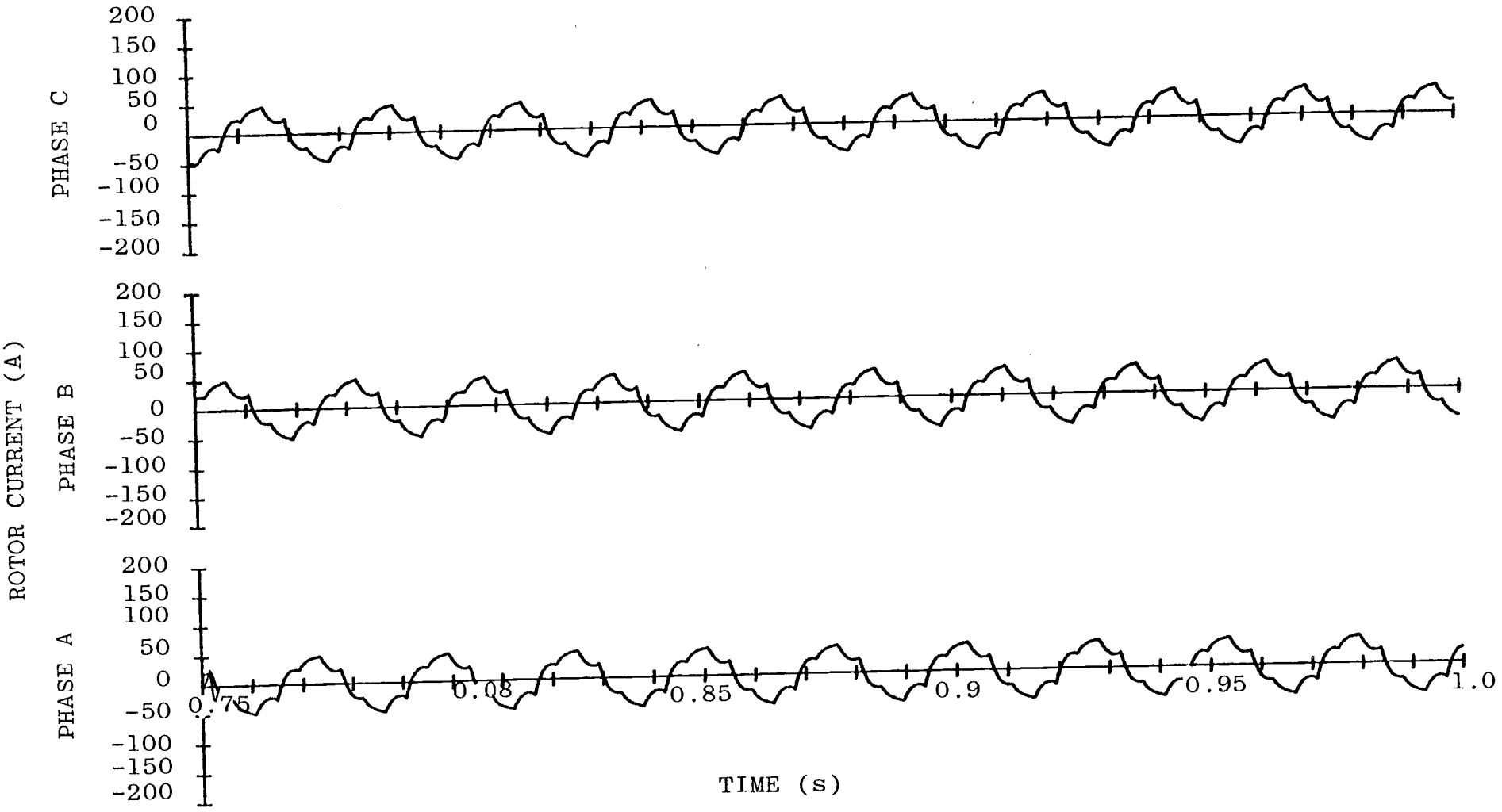

Figure 21. Rotor Current Referred to the Stator During Closed Loop Operation.

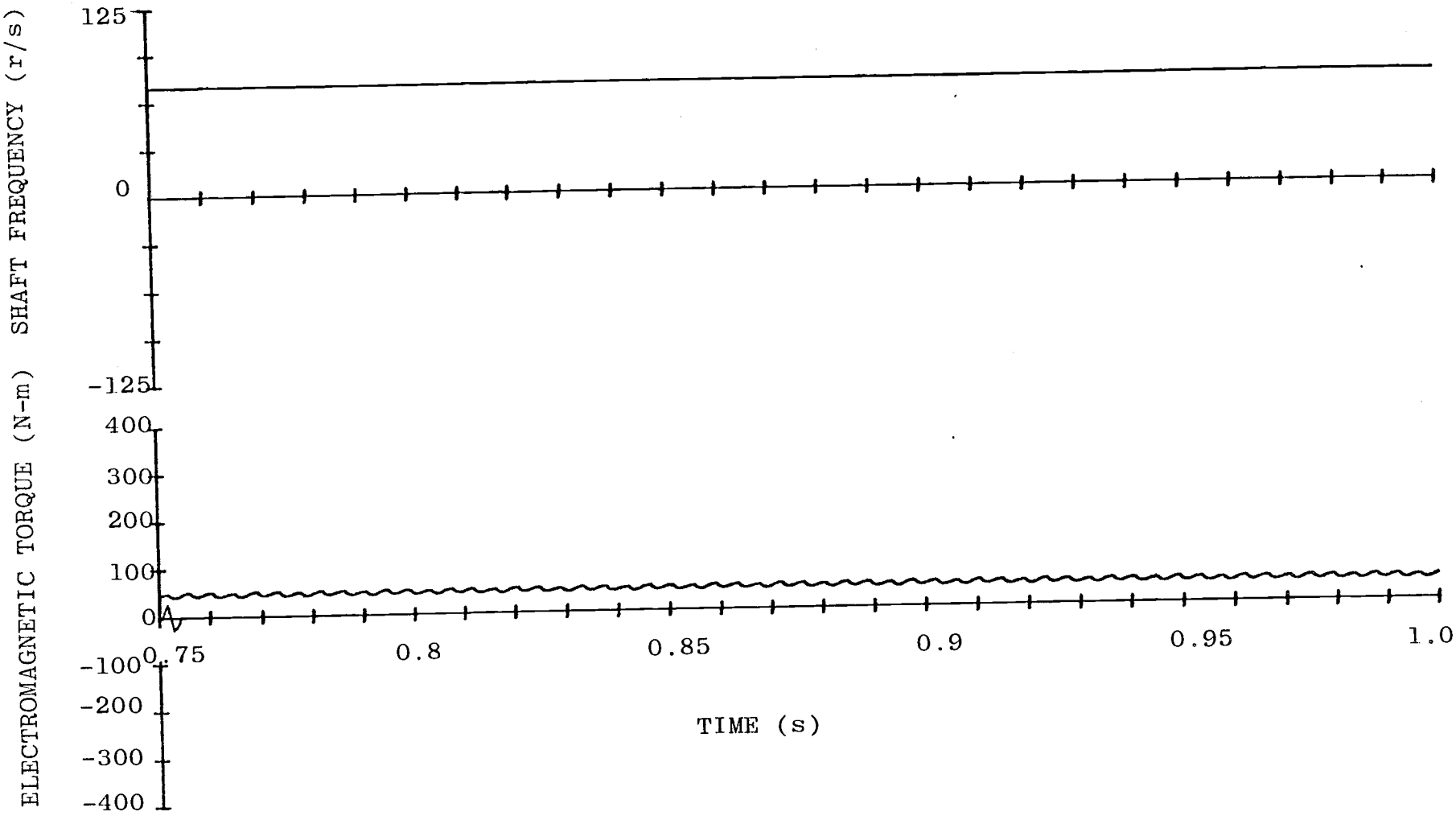

Figure 22. Electromagnetic Torque and Shaft Frequency During Closed Loop Operation.

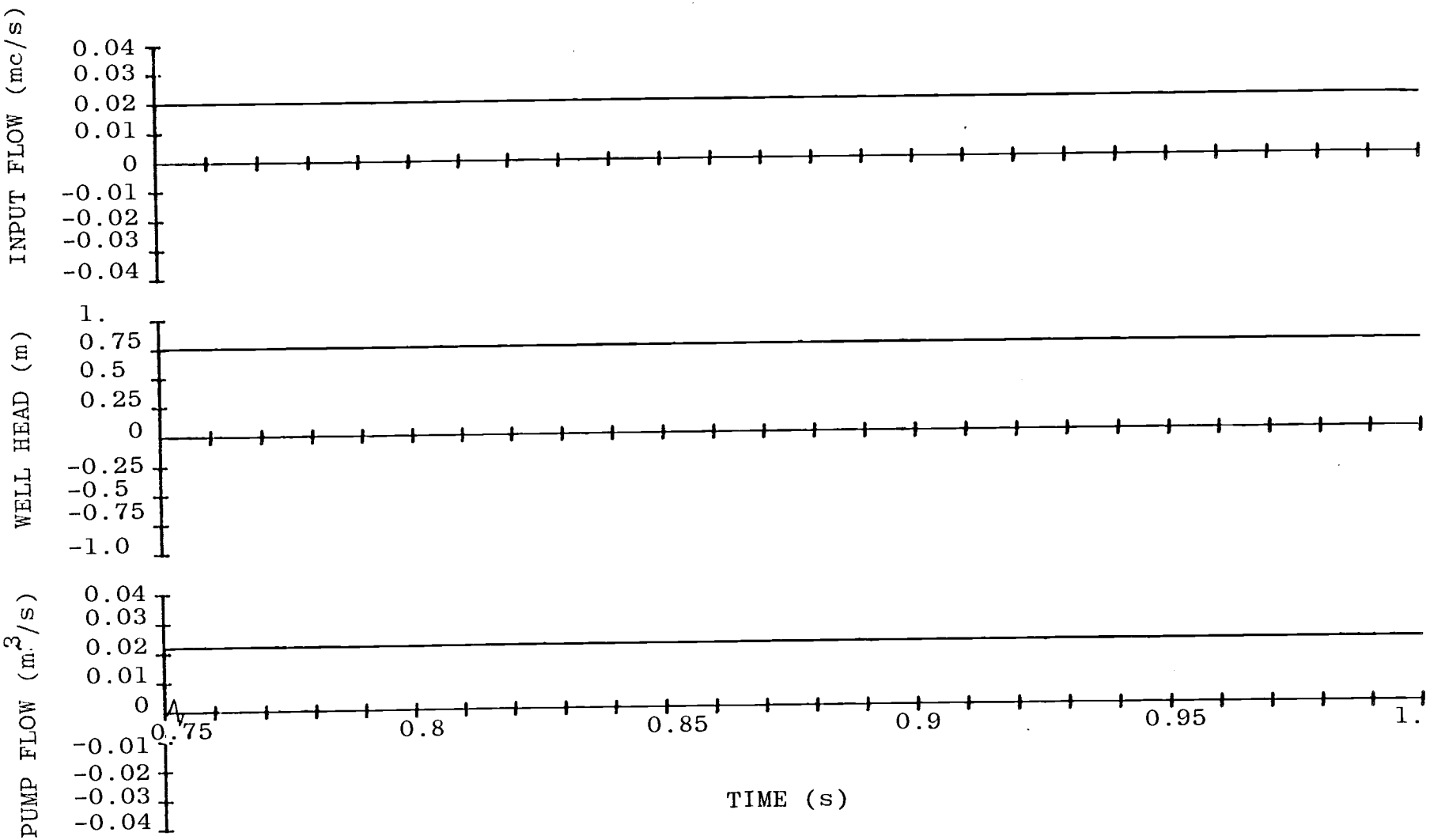

Figure 23. Pump Flow, Well Head, and Input Flow During Closed Loop Operation.

Frequency Response Analysis

Open loop and closed loop perturbation system transfer functions are evaluated as follows [6].

For the discrete dynamic elements, the system state perturbations at a given time instant are described by

$$x_{k+1} = \phi x_k + \psi u_{k+1}$$

$$y_k = Cx_k$$

For x (0) = 0, the system transfer function is given by

$$\frac{y_i}{u_j} = C_i(\ zI-A)^{-1}B_j$$

where i denotes the ith row of C and j denotes the jth column of B.

The coefficients of the numerator and denominator polynomials of $\frac{y_i}{u_j}$ are determined using Leverrier's algorithm [6] which is a procedure for determining simultaneously the coefficients of the characteristic polynomial of a matrix.

The transfer functions evaluated are output shaft frequency per input voltage and output shaft frequency per input frequency. These transfer functions are evaluated for the feedback gains open and closed. The

open loop transfer functions are given by

$$\frac{\omega_m}{v_m} = C_5(sI - A)^{-1} B_1$$

where $C_5 = [0 \quad 0 \quad 0 \quad 0 \quad 1 \quad 0 \quad 0]$

$$B_1 = \begin{bmatrix} \frac{l_r}{d} \ 1.5 \cos\theta \\ -\frac{l_r}{d}(1.5\cos\theta + 1.299\sin\theta) \\ -\frac{l}{d} \ 1.5\cos\theta \\ \frac{l}{d}(0.75\cos\theta + 1.299\sin\theta \end{bmatrix}$$

$$\frac{\omega_m}{\omega_s}(s) = C_5 (sI - A)^{-1} B_2$$

$$B_2 = \begin{bmatrix} -\frac{V\,T\,l_r}{d} \ 1.5\sin\theta \\ \frac{V\,T\,l_r}{d}(0.75\sin\theta - 2.165\cos\theta) \\ -\frac{V\,T\,l_m}{d} \ 1.5\sin\theta \\ \frac{V\,T\,l_m}{d}(-0.75\sin\theta + 2.165\cos\theta) \end{bmatrix}$$

Open and closed loop pole placements in the Z-plane obtained at t = 0.5 s for the case previously described are shown in Figure 24.

Summary

The design of the perturbation feedback control law was accomplished using a quadratic penalty function in the state and control. A recurrence relation for the steady state gains was evaluated at the switching points in the power supply waveform. The gain equation converged in five iterations on the first cycle of feedback control and subsequently converged in one iteration for the particular conditions simulated. The closed loop control system indicated a slight tendency to generate a limit cycle in the command power supply frequency as evidenced by Figure 18. Comparison of Figures 16 and 22 indicates that the limit cycle in the command does not significantly affect the amplitude of the torque pulsation during steady state operation. The closed loop system is clearly stable, as evidenced by simulation results and by closed loop pole placement as shown in Figure 24.

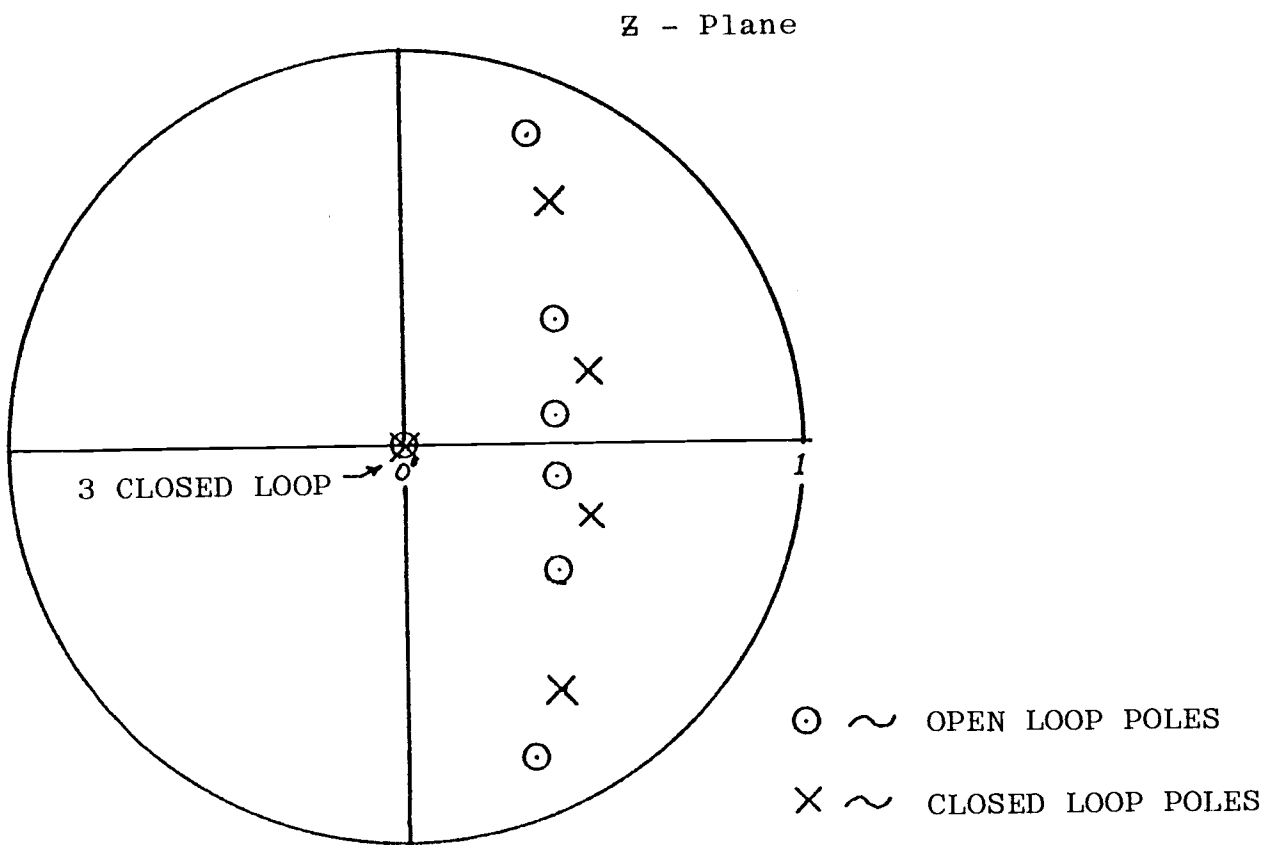

Figure 24. Open and Closed Loop Perturbation Control System Pole Placement.

IV. SUMMARY AND CONCLUSIONS

Summary

A mathematical model of a sewage pumping station has been developed and used in the design and evaluation of a perturbation feedback control system. The control system gains are calculated at each sample instant using linear quadratic control theory results. A simulation of the system has been used to evaluate the open loop starting characteristics of the system and the steady state operation of the closed loop controller. The open and closed loop system pole placement was calculated and shows that the perturbation control system is stable.

Conclusion

Results presented in the preceding chapters indicate that a pertubation feedback control system designed using linear quadratic optimal control theory is a feasible method for improving the short period performance of a variable frequency induction motor drive for a centrifugal pump. The role of simulation in the approach to this problem is significant for a number of reasons. First, the system model is complicated by the nonlinearity of both the motor and power supply and the pump. Second, the relationship between the values of the weighting matrices in the cost function and the control system

performance is imprecisely defined. The simulation of the system plays a central role in adjusting the cost function parameters to obtain suitable closed loop system performance. Third, there is no a-priori assurance that the first order perturbations about a nominal system operating point will adequately represent the behavior of the system; the simulation of the system affords a method to verify the validity of this approach and to assess the sensitivity of the system performance to uncertainty in the nominal system operating point and characteristics.

Recommendations for Further Research

The assumptions embodied in the power supply model result in an inherently stable open loop operating condition for the system. It has been shown [5], [12] that source impedance can have a deleterious effect on operating point stability, particularly at low excitation frequencies.

An evaluation of closed loop control to stabilize these inherently unstable operating points is therefore recommended. Simplifying assumptions in the modeling of the pump and hydraulic subsystem might also be relaxed in further research on this topic; in particular the assumptions of constant fluid mass required to be accelerated by the pump and constant static head. One other area of potential interest is consideration of the estimation/state reconstruction aspects of this problem. The potential benefits

are twofold: first, the required number, type, and accuracy of sensors could be evaluated systematically; and second, a stochastic estimator would provide the mechanism to estimate the fundamental driven states of the system by treating the effect of neglected harmonics as disturbances.

BIBLIOGRAPHY

1. J. M. D. Murphy, Thyristor Control of A. C. Motors, Pergamon Press, New York, 1973.

2. Ronald E. Bartlett, Pumping Stations for Water and Sewage, John Wiley and Sons, New York, 1974.

3. James B. Rishel, Robert H. Endejann, "Variable Speed Pumping Minimizes Energy Usage", Consulting Engineer (St. Joseph, Mich) Vol. 4'2 no. 5, May 1974.

4. Charles R. Hollis, "Review of Five Types of Electrical Adjustable Speed Drives and Their Application to a Centrifugal Pump", IEEE Industrial Applications Society, Annual Meeting, Eighth Conference Record Papers, Milwaukee, Wisconsin, October 8-11, 1973.

5. Thomas A. Lipo, Paul C. Krause, "Stability Analysis of a Rectifier--Inverter Induction Motor Drive," IEEE Transactions on Power Apparatus and Systems, Vol. PAS-88, No. 1, January 1969.

6. Huibert Kwakernak, Raphael Sivan, Linear Optimal Control Systems, Wiley-Interscience, New York, 1972.

7. Michael Athans, "The Role and Use of the Stochastic Linear--Quadratic-Gaussian Problem in Control System Design", IEEE Transactions on Automatic Control Vol. AC-16, No. 6, December 1971.

8. Stuart D. T. Robertson, Kattingeri M. Hebbar, "A Digital Model for Three-Phase Induction Machines", IEEE Transactions on Power Apparatus and Systems, Vol. PAS-88, No. 11, November 1969.

9. A. J. Stepanoff, Centrifugal and Axial Flow Pumps, John Wiley and Sons, Inc., New York, 1948.

10. A. E. Fitzgerald, Charles Kingsley, Jr., Electric Machinery, McGraw Hill, New York, 1952.

11. J. S. Meditch, Stochastic Optimal Linear Estimation and Control, McGraw-Hill Book Co., New York, 1969.

12. T. A. Lipo, A. B. Plunkett, "A Novel Approach to Induction Motor Transfer Functions", IEEE Transactions on Power Apparatus and System, Vol. PAS-90, No. 5, September/October 1974.

APPENDIX A

INDUCTION MACHINE PARAMETER ESTIMATION

Introduction

On March 25 and 26, 1976, data were taken on a 3-phase 6-pole 15 HP wound rotor induction machine in the OSU power lab at various steady-state operating conditions. Data were taken at 3 no load operating conditions and at 6 operating conditions under load. Additionally, data were taken to allow determination of the relative calibration of some of the instrumentation used in the experiment.

The following sections summarize the experiment configuration, and present in tabulated form the instrument readings obtained during the various tests.

Test Configuration

The test involved the a.c. (induction) machine, a direct coupled d.c. machine operating as a motor or generator depending on the test, a.c., and d.c. power taken from shop set 2 and a resistive load for the d.c. generator. A pictorial sketch of the layout of the two machines is shown in Figure A-1.

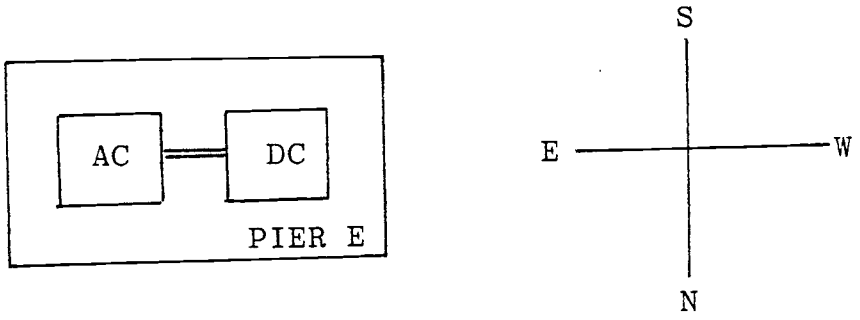

Figure A-1. Plan view of machine pier.

The nameplate data for the a.c. and d.c. machines are shown in Tables A-1 and A-2 respectively.

Table A-1. a.c. machine.

Westinghouse Wound Rotor Motor
Serial 7309
3-phase
60 HZ
15 HP
1140 RPM
230/460 Volts
42/21 AMP

Table A-2. d.c. machine.

Diehl d.c. Motor-Generator
No. 439498
E. S. No K7-108
250 volts
50 AMP
20 HP
Type K7
700/2100 RPM
Shunt Field

No Load Tests

No load test data were taken for the rotor windings of the a.c. machine open circuit at 0 rotor angular frequency, at $-\omega_s$ angular frequency and $+\omega_s$ rotor angular frequency where ω_s = synchronous frequency and positive rotation is counterclockwise when viewed from west to east (see Figure A-1). For these 3 sets of data, the test circuits were as shown in the following figures.

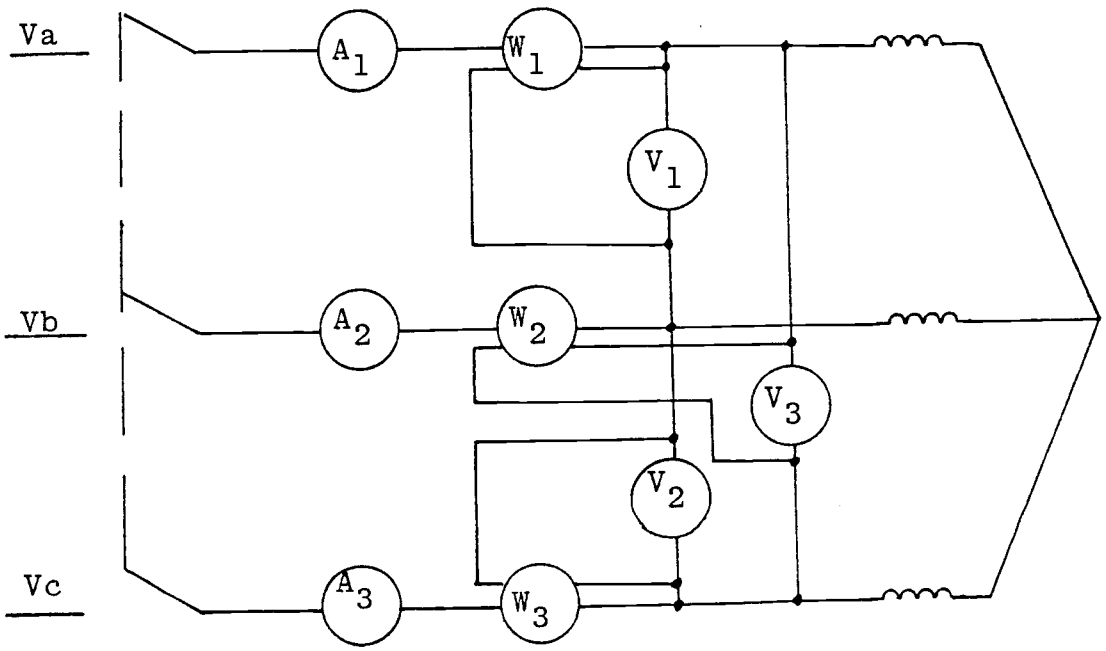

Figure A-2. A.c. Machine Stator Instrumentation Circuit Diagram.

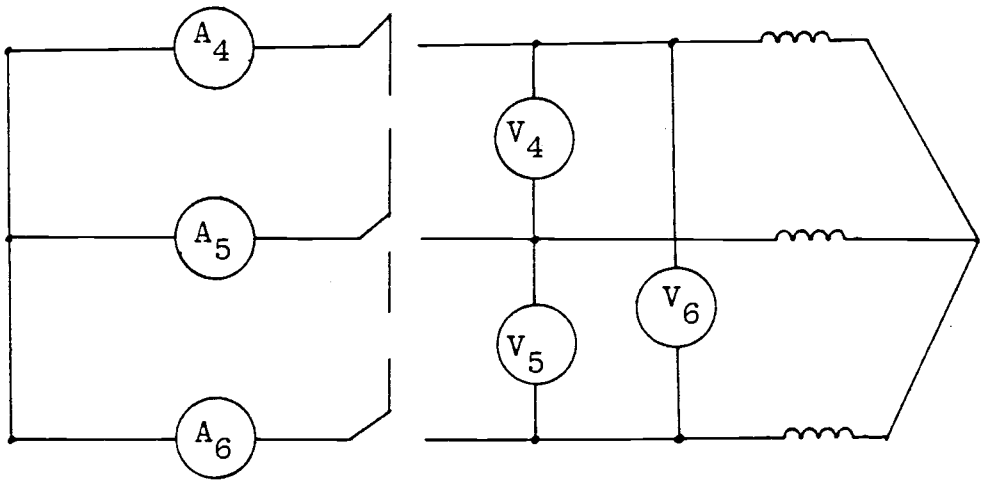

Figure A-3. A.c. Machine Rotor Instrumentation Circuit Diagram.

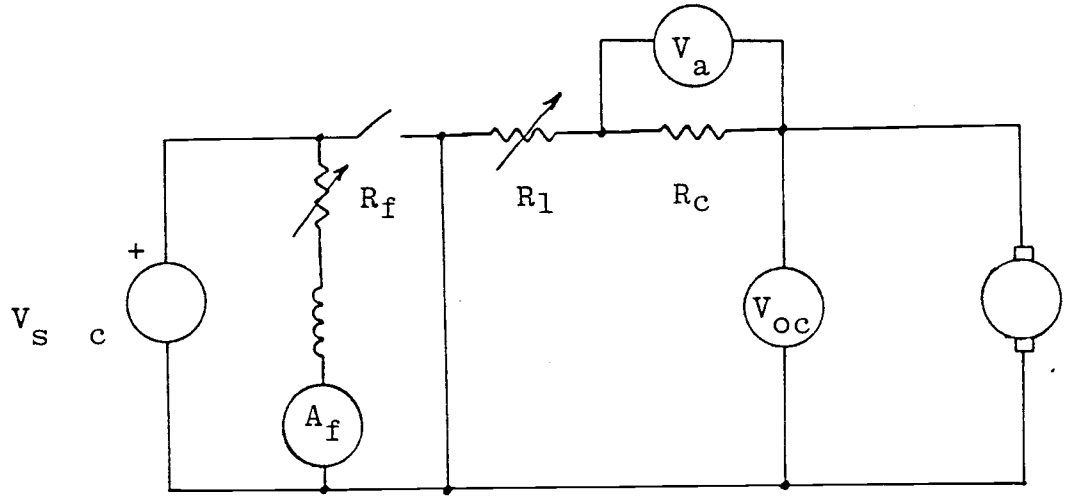

Figure A-4. D.c. Machine Instrument Circuit Diagram.

Data were first taken with a multimeter to determine the d.c. resistance of the various windings with the terminals in Figure A-2 labelled a, b, c, from east to west for the stator and rotor respectively, the following data were obtained.

Table A-3. Multimeter Data (OSU No. 94672).

Stator	
R_{ab}	= 0.23
R_{bc}	= 0.23
R_{ac}	= 0.23
Rotor	
R_{ab}	= 6.0
R_{bc}	= 4.3
R_{ac}	= 4.3

Three sets of data were taken under no load conditions; one with the rotor at standstill and two with the rotor at synchronous speed. To obtain synchronous speed, the d.c. machine was used as a motor to supply the torque required to overcome friction and windage. The rotor line-to-line voltage was monitored using an oscilloscope, and the speed of the rotor was adjusted using R_F (see Figure A-4) such that the rotor voltage amplitude was minimized. In all cases, the rotor circuits were open (see Figure A-3). Data

for the no load test are presented in Tables A-4, A-5, A-6, and A-7.

Parameter Estimation

Estimates of the values of the wound rotor induction machine parameters are obtained as follows. The machine equivalent circuit, shown in Figure A-8, is used to obtain equations which relate measured quantities to the unknown parameters. The open circuit test data is used to obtain values for the combined stator impedence and magnetizing impedence. These values are used to eliminate two of the unknowns from the circuit equations. The remaining unknowns are then determined using a least squares fit of the parameters to the load test data.

Impedence from No Load Test Data

The machine equivalent circuit under no-load conditions is shown in Figure A-9. Using data from Table A-7, data point 6, the open circuit impedance of the machine after instrument correction, is

$$z_{oc} = 0.9156 + j\ 9.429 \text{ ohms.}$$

Load Test Data Analysis

The phasor equations obtained from the machine equivalent circuit are given by

Table 4. No-load Test Instruments.

	Range (S)	Serial	Shunt Res. OHMS
V_1	0-150/300 V (0.7 V high at 130V, rest - 0.1 V)	334514	1813/3626
V_2	0-150/300 V (0.2 V high at 140, 150V, rest - 0.1V)	334513	1717/3437
V_3	0-150/300 V (within 0.1 V)	3219291	1985/3970
V_4	0-300/750 V (within 0.2V)	598915	7614/19040
V_5	0-150/300V (within 0.1 V)	3219290	2038/4077
V_6	0-150/300 V (0.25 high above 120V, rest 0.1)	3320366	2027/4055
A_1	0-5a	577759	N/A
A_2	0-5a	584737	N/A
A_3	0-5a	3320349	N/A
W_1	0-150 W; 0-100/200 V (0.1 W) 5/10a	3217509	2359/4718
W_3	0-150 W; 0-100/200 V (0.1 W) 5/10a	3217510	2370/4741
W_2	0-250 W; 0-50/100/200 V (0.2 W) 5/10a	3327789	2348/4770/9541

Table A-5 Zero Rotor Frequency No Load Data

	V_1	CALIB	SF	$\hat{V}_1$	V_2	CALIB	SF	$\hat{V}_2$	V_3	CALIB	SF	$\hat{V}_3$
1	40.0		1		40.7		1		40.7		1	
2	60.4				60.7				60.9			
3	79.4				80.1				79.8			
4	79.6				79.8				80.0			
5	101.1				101.3				101.3			
6	120.3				120.5				120.5			
7	140.9				141.0				140.6			
8	75.8		2		75.7		2		76.6		2	
9	75.8				75.9				76.6			
10	90.3				90.3				90.8			
11	100.0				100.1				100.4			
12	109.8				110.0				110,3			

	V_4	CALIB	SF	$\hat{V}_4$	V_5	CALIB	SF	$\hat{V}_5$	V_6	CALIB	SF	$\hat{V}6$
1	45		1		42.2		1		44.2		1	
2	69				66.8				66.2			
3	88				87.1				86.9			
4	89				87.0				88.0			
5	112.2				111.2				110.3			
6	132.5				132.0				131.2			
7	154.0				76.6		2		76.7		2	
8	168.0				83.5				83.4			
9	168.0				84.1				83.7			
10	199.5				99.5				99.4			
11	219.0				110.2				109.8			
12	239.0				120.0				120.0			

Note: $\hat{V}_1 = (V_1 + \text{CALIB}) \times \text{SF}$ (TYPICAL)

Table A-5, (cont.)

	A_1	CALIB	TR	$\hat{A}_1$	A_2	CALIB	TR	$\hat{A}_2$	A_3	CALIB	TR	$\hat{A}_3$
1	2.60		1		2.55		1		2.61		1	
2	3.81				3.81				3.82			
3	4.97				4.98				4.94			
4	2.51		2		2.46		2		2.51		2	
5	3.15				3.16				3.18			
6	3.78				3.78				3.80			
7	4.49				4.53				4.52			
8	4.95				5.02				5.02			
9	2.01		5		2.00		5		2.06		5	
10	2.60				2.60				2.68			
11	3.24				3.28				3.32			
12	4.42				4.46				4.50			

NOTE: $\hat{A}_1 = (A_1 + \text{CALIB}) \times \text{TR}$, etc.

	W1	CALIB	SF	TR	$\hat{W}1$	W2	CALIB	SF	TR	$\hat{W}_2$	W_3	CALIB	SF	TR	$\hat{W}_3$
1	-34.4		1	1		101.2		1	1		68.8		1	1	
2	-81.7					227.0					78.9		2		
3	-141					195.0		2			128.4				
4	-68			2		98.0			2		63.1			2	
5	-113.3					157.5					102.2				
6	-83.3			2		223.0					147.0				
7	-117.2					156.0		4			101.0		4		
8	-145.2					190.2					119.8				
9	-59.6			5		76.0			5		50.3			5	
10	-91.0					119.0					72.8				
11	-129.5					162.5					101.8				
12	-100.4		4			242.					151.0				

NOTE: $W_1 = (W_1 + \text{CALIB}) \times \text{SFXTR}$, etc.

Table A-6. Synchronous Rotor Frequency Data (Clockwise Rotation).

	V_1	CALIB	SF	$\hat{V}_1$	V_2	CALIB	SF	$\hat{V}_2$	V_3	CALIB	SF	$\hat{V}_3$
1	111.2		2		111.3		2		111.8		2	
2	100.3				100.9				101.1			
3	90.1				90.7				90.9			
4	80.3				80.9				81.1			
5	140.5		1		141.2		1		141.2		1	
6	120.3				121.0				121.1			
7	100.1				100.8				100.8			
8	79.8				80.2				80.5			
9	80.0				81.2				81.1			
10	60.0				60.4				60.8			
11	40.3				40.7				40.8			

	A_1	CALIB	TR	$\hat{A}_1$	A_2	CALIB	TR	$\hat{A}_2$	A_3	CALIB	TR	$\hat{A}_3$
1	4.44		5		4.46		5		4.45		5	
2	3.16				3.20				3.22			
3	2.54				2.53				2.62			
4	2.13				2.12				2.14			
5	4.42		2		4.46		2		4.43		2	
6	3.72				3.75				3.73			
7	3.06				3.08				3.09			
8	2.46				2.44				2.47			
9	4.90		1		4.94		1		4.88		1	
10	3.65				3.68				3.69			
11	2.50				2.46				2.50			

Table A-6, (cont.)

	W_1	CALIB	SF	TR	W_1	W_2	CALIB	SF	TR	W_2	W_3	CALIB	SF	TR	W_3
1	-109.5		4a	5		246		4v	5		145.2		4a	5	
2	-137.0		2v			160.5					94.2				
3	-98.8					114.2					135.0		2v		
4	-73.5					86.0					100.2				
5	-129.2			2		156.			2		92.8		4	2	
6	-95.0					224.		2v			135.8		2v		
7	-126.8		1v			154.					94.2				
8	-82.2					98.					116.2		1a		
9	-79.5		2a	1		199.			1		120.0		2a	1	
10	-89.1		1			221.		1v			135.		1a		
11	-42.0					98.5					61.9				

Table A-7. Synchrononous Rotor Frequency Data(Counter-clockwise Rotation).

	V_1	CALIB	SF	$\hat{V}_1$	V_2	CALIB	SF	$\hat{V}_2$	V_3	CALIB	SF	$\hat{V}_3$
1	40.3		1		40.9		1		41.0		1	
2	60.8				6.10				61.0			
3	80.3				81.6				81.7			
4	80.0				80.8				80.9			
5	99.9				100.3				100.3			
6	120.4	1.006		121.1	121.0	1.003		121.4	121.2	1.000		121.2
7	139.0				139.6				139.2			
8	80.0		2		80.6		2		80.9		2	
9	90.1				90.9				91.0			
10	100.0				100.8				100.9			
11	110.6				111.2				111.2			
	334514				334513				3219291			

	A_1	CALIB	TR	$\hat{A}_1$	A_2	CALIB	TR	$\hat{A}_2$	A_3	CALIB	TR	$\hat{A}_3$
1	2.52		1		2.50		1		2.52		1	
2	3.69				3.75				3.71			
3	4.90				4.99				4.91			
4	2.45		2		2.43		2		2.45		2	
5	3.03				3.07				3.05			
6	3.68	1.004		7.39	3.72	0.999		7.43	3.70	0.999		7.39
7	4.30				4.36				4.29			
8	2.08		5		2.07		5		2.09		5	
9	2.50				2.50				2.51			
10	3.09				3.15				3.12			
11	4.34				4.40				4.33			
	577759				584737				3320349			

Table A-7, (cont.)

	W_1	CALIB	SF	TR	W_1	W_2	CALIB	SF	TR	W_2	W_3	CALIB	SF	TR	W_3
1	-37.4		1	1		102		1	1		64.8		1	1	
2	-85.8					227					137.2				
3	-78.7		2a			202		2a			120.0		2a		
4	-78.2		1	2		197		1	2		118.0		1	2	
5	-123.0					152		2v			93.0		2v		
6	-87.2		2v			222					133.0				
7	-117.6					150		4v			88.2		4a		
8	-66.1			5		83.5			5		97.1		2a	5	
9	-91.2					113.5					130.4				
10	-131.6					158.					91.3		4a		
11	-100.7		4a			241.					136.7				
	3217509					3327789					3217510				

Load Test.

Load test data were taken by using the d.c. machine as a generator and varying R_L (See Fig. A-4). All load test data were obtained for counterclockwise rotation. Data are shown in tables A-8 and A-9.

Table A-8

Load Test Instruments

	RANGE(S)	NO.
V_1	See Table 4	334514
V_2		334513
V_3		3219291
A_1		577759
A_2		584737
A_3		3320349
A_4	0-5a	3217500
A_5	0-5a	3320348
A_6	0-5a	3217501
W_1	0-500; 0-150/300v (30v) 0-5/10a	309769
W_2	0-500; 0-150/300v 0-5/10a	638341
W_3	0-500; 0-150/300v 0-5110a	301502
R_c		3326
V_A	0-200mv	576884
Vdc	0-150/300vd.c.	586496
A_F	0-5a	3204263
STROBE		GR 1531-AB STROBOTAC

Table A-9. Load Test Data

	V_1	CALIB	SF	$\hat{V}_1$	V_2	CALIB	SF	$\hat{V}_2$	V_3	CALIB	SF	$\hat{V}_3$
1	120.0	1.006	1	120.7	120.8	1.003	1	121.2	120.8	1.000	1	120.8
2	120.0			120.7	120.2			120.6	119.6			119.6
3	120.0			120.7	120.6			121.0	120.7			120.7
4	120.0				121.0				120.9			
5	120.0			120.7	120.8			121.2	121.1			121.1
6	100.0	1.005		100.5	100.2	1.005		100.7	100.4	1.002		100.6
	334514				334513				3219291			

	A_1	CALIB	TR	$\hat{A}_1$	A_2	CALIB	TR	$\hat{A}_2$	A_3	CALIB	TR	$\hat{A}_3$
1	4.25	0.999	5	21.23	4.26	0.994	5	21.17	4.46	1.003	5	22.37
2	3.80	1.001		19.02	3.80	0.998		18.96	3.95	1.001		19.77
3	3.25	1.003		16.30	3.28	1.000		16.40	3.44	0.9975		17.16
4	2.79				2.72				2.90			
5	4.35	0.999*	2	8.69	4.32	0.995*	2	8.60	4.42	1.003*	2	8.87
6	4.05	0.999*		8.09	3.96	0.997*		7.90	4.11	1.002*		8.24
	577759				584737				3320349			

	A_4	CALIB	TR	$\hat{A}_4$	A_5	CALIB	TR	$\hat{A}5$	A6	CALIB	TR	$\hat{A}6$
1	3.18	.997	5		2.98	1.00	5		3.05	1.003	5	
2	2.80				2.55				2.58			
3	2.28				2.14				2.17			
4	3.67		2		3.37		2		3.53		2	
5												
6												

*Values for TR = 1

Table A-9 (cont)

	W_1	CALIB	SF	TR	$\hat{W}_1$	W_2	CALIB	SF	TR	$\hat{W}_2$	W_3	CALIB	SF	TR	$\hat{W}_3$
1	218		1	5	1090	258		1	5	1290	275		2a	5	2750
2	190				950	237				1185	242				2420
3	147				735	214				1070	410		1		2050
4	98				490	211				1055	345				1725
5	-5			2	-10	442			2	884	475			2	950
6	45				90	306				612	390				780

	V_a	SF	$\hat{V}_a$	V_{dc}	SF	$\hat{V}_{dc}$	AF	SF	$\hat{AF}$	W_m
1	38.5	0.2	7.7amp	257	1		0.86	1		1100
2	33.2		6.64	261			0.86			1122
3	26.0		5.20	264			0.86			1140
4	18.0		3.60	262			0.86			1127
5	0.0		0	276			0.85			1172
6	0.0		0	274			0.86			1168

NOTE: W_m = Shaft frequency measured with strobotac.

Instrument Calibration

Instrument calibration data were taken for circuits as shown in the following figures.

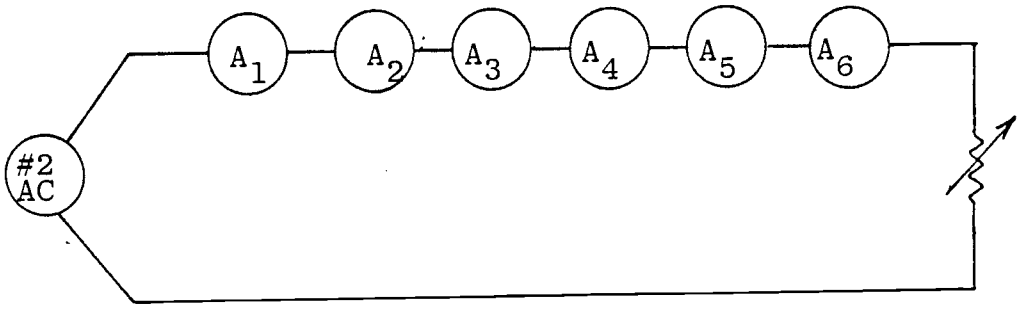

Figure A-5. Ammeter Calibration Circuit.

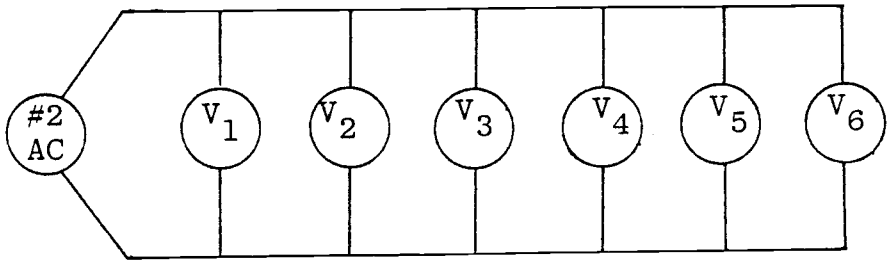

Figure A-6. Voltmeter Calibration Circuit.

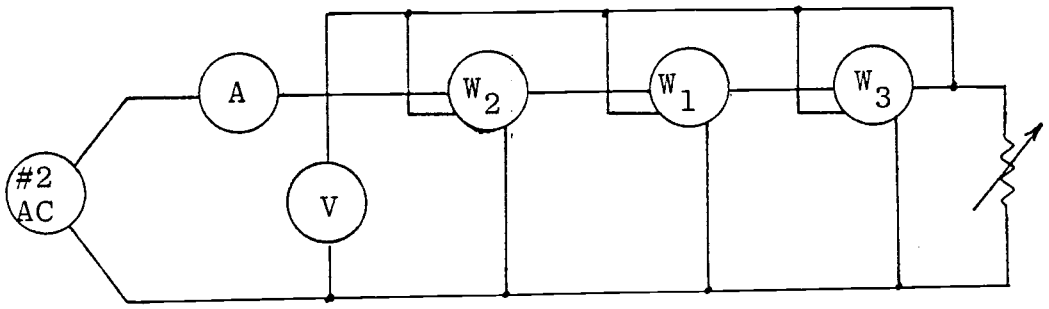

Figure A-7. Wattmeter Calibration Circuit.

Data are shown in the table.

Table A-10. Instrument Calibration Data

	TR	A	CALIB*	A_2		A_3		A_4		A_5		A_6		A
1	5	4.92	0.997	4.95	0.991	4.89	1.003	4.95	0.991	4.87	1.008	4.86	1.010	4.91
2		4.49	0.999	4.52	0.992	4.46	1.005	4.53	0.990	4.46	1.005	4.44	1.010	4.483
3		3.99	0.999	4.00	0.996	3.98	1.001	4.01	0.994	3.97	1.004	3.96	1.006	3.985
4		3.50	1.003	3.51	1.000	3.52	0.998	3.54	0.992	3.51	1.000	3.49	1.006	3.512
5		2.99	1.003	3.00	1.000	3.01	0.997	3.01	0.997	3.00	1.000	2.99	1.003	3.000
6		2.50		2.46		2.51		2.48		2.49		2.50		
7		1.99		1.95		1.98		1.96		1.97		1.97		
8		1.48		1.44		1.48		1.43		1.46		1.47		
9		1.07		1.05		1.08		1.05		1.07		1.08		
10	10	3.49		3.51		3.52		3.53		3.51		3.51		
11	20	3.50		3.52		3.53		3.54		3.51		3.51		
12	2	3.45	1.004	3.47	0.999	3.47	0.999	3.48	0.996	3.46	1.001	3.46	1.001	3.465
13	1	4.97		4.96		4.90		4.97		4.89		4.88		
14		4.47	0.999	4.50	0.993	4.45	1.004	4.51	0.990	4.44	1.006	4.43	1.008	4.467
15		4.01	0.999	4.02	0.997	4.00	1.002	4.04	0.992	3.99	1.004	3.98	1.007	4.007
16		3.49		3.50		3.51		3.53		3.49		3.49		
17		2.99		3.00		3.00		3.01		3.00		2.99		
18		2.53		2.49		2.52		2.52		2.52		2.52		
19		2.04		2.01		2.04		2.01		2.01		2.03		
20		1.49		1.43		1.48		1.43		1.46		1.46		
21		1.05		1.02		1.05		1.00		1.01		1.03		
		577759		584737		3320349		3217500		3320348		3217501		

* READING X CALIB = VALUE

Table A-10, (cont.)

	V_1		V_2		V_3		V_4		V_5		V_6		$\bar{V}$
1	149.0		149.2		149.1		149.0		149.8		150.0		
2	139.6		140.0		140.0		139.7		140.3		140.4		
3	129.4		129.9		130.1		130.3		130.6		130.2		
4	119.2	1.006	119.6	1.003	120.0	1.000	120.1	0.999	120.9	0.992	119.9	1.000	119.95
5	110.0		110.2		110.8		111.2		111.3		110.5		
6	99.7	1.005	99.7	1.005	100.0	1.002	100.7	0.995	101.1	0.991	99.8	1.004	100.17
7	90.6		90.7		91.1		91.0		90.9		90.9		
8	80.0		80.3		80.9		80.4		80.4		80.5		
9	70.1		70.2		70.8		70.3		70.6		70.4		
10	60.1		60.1		60.7		61.5		61.1		60.5		
11	50.0		50.0		50.5		50.0		50.9		50.1		
12	39.8		40.0		40.1		41.1		39.5		39.5		
	334514		334513		3219291		598915		3219290		3320366		

	A		V		W_2		W_1		W_3			
1	4.24		112.7		466		467		480			
2	3.54		113.1		406		404		405			
3	3.03		113.4		347		346		347			
4	2.67		113.7		305		304		304			
5	2.17		114.1		245		247		247			
6	1.94		102.5		197		199		198			
7	1.46		88.2		145		147		146			
8	1.37		73.3		100		100		101			
9	1.27		41.0		50		50		51			
10			102.7		17		16		16			
	3217501		334513		638341		309769		301502			

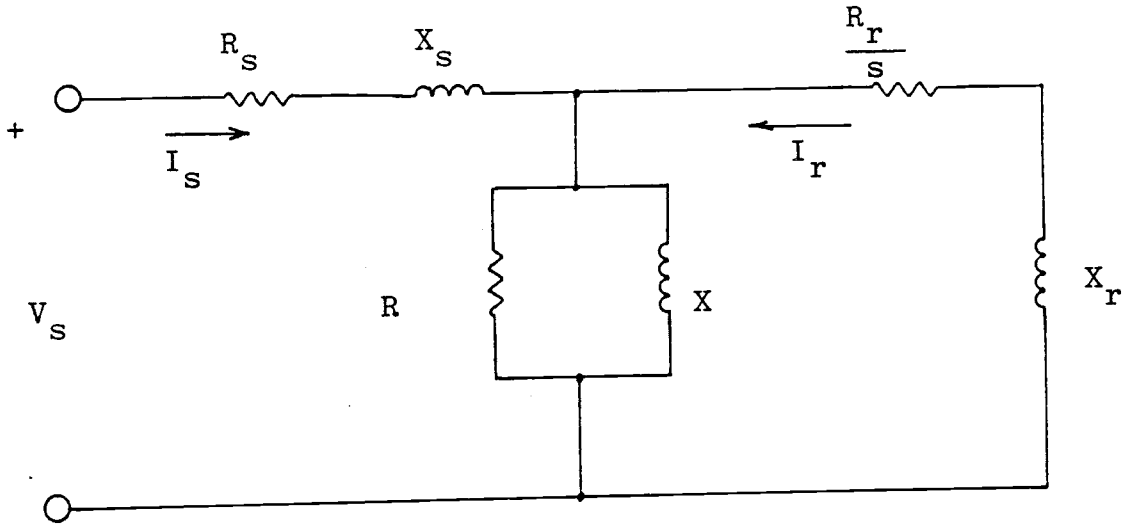

Figure A- 8. Induction Machine Equivalent Circuit.

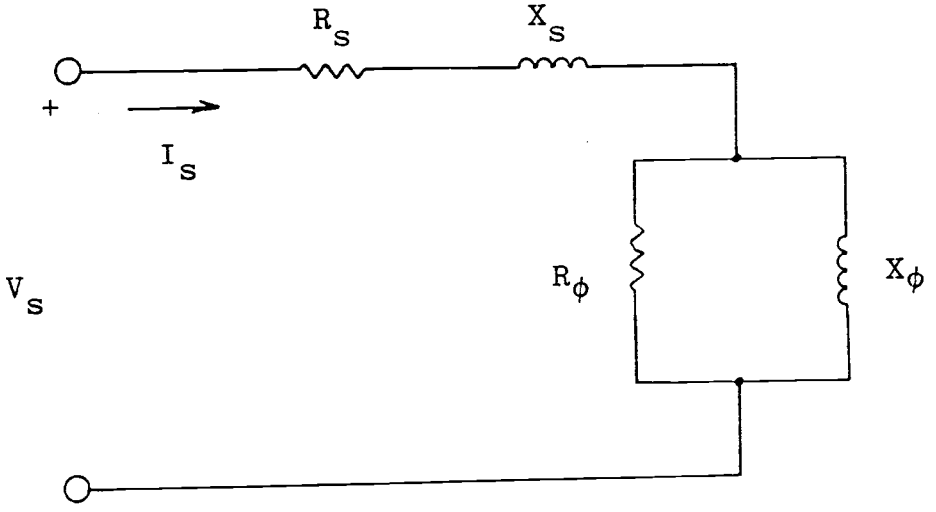

Figure A-9. Stator Equivalent Circuit (No-Load)

$$V_s = I_s Z_s + (I_s + I_R) Z_m$$

$$0 = I_s Z_m + I_R (Z_R + Z_m)$$

where Z_m is the series equivalent impedence of the magnetizing branch. Using

$$Z_{oc} = Z_s + Z_m$$

results in

$$V_s = Z_{oc} I_s + Z_m I_R$$

$$0 = Z_m I_s + (Z_R + Z_m) I_R$$

The objective is to obtain values for Z_m, Z_R, Z_s, and I_R given V_s and I_s at various values of load and Z_{oc} obtained from the open circuit data. Rewriting the circuit equations in terms of the unknowns and expanding complex values into real and imaginary components results in the following equation:

$$\begin{bmatrix} V_s & -R_{oc} I_{sa} + X_{oc} I_{sb} \\ -R_{oc} I_{sb} & -X_{oc} I_{sa} \\ 0 & \\ 0 & \end{bmatrix}$$

$$= \begin{bmatrix} I_{Ra} & -I_{Rb} & 0 & 0 \\ I_{Rb} & I_{Ra} & 0 & 0 \\ I_{sa}+I_{Ra} & -I_{sb}-I_{Rb} & -I_{Rb} & I_{Ra} \\ I_{sb}+I_{Rb} & I_{sa}+I_{Ra} & I_{Ra} & I_{Rb} \end{bmatrix} \begin{bmatrix} R_m \\ X_m \\ X_R \\ R_R \end{bmatrix}$$

which is written in vector-matrix notation as

$$y = hx$$

As the rotor currents are unknown, the preceding equation is non-linear. This equation is linearized by augmenting the state vector with perturbations in the rotor currents and taking the partial derivative of the h-matrix with respect to rotor currents. The linearized system is given by the following equation

$$y = \begin{bmatrix} I_{Ra} & -I_{Rb} & 0 & 0 & R_m & -R_m \\ I_{Rb} & I_{Ra} & 0 & 0 & X_m & R_m \\ I_{sa}+I_{Ra} & -I_{sb}-I_{Rb} & -I_{Rb} & +I_{Ra} & R_m+R_R & -X_m-X_R \\ I_{sb}+I_{Rb} & I_{sa}+I_{Ra} & I_{Ra} & I_{Rb} & X_m+X_R & R_m+R_R \end{bmatrix} \begin{bmatrix} R_m \\ X_m \\ X_R \\ R_R \\ \delta I_{Ra} \\ \delta I_{Rb} \end{bmatrix}$$

or

$$Y = HX$$

For each value of load, four measurements are obtained. The three constant parameters R_m, X_m, and X_R constitute three unknowns and the other three parameters R_R, δI_{Ra}, and δI_{Rb} constitute three additional unknowns for each value of load. A system of equations, obtained by concatenating the linearized system of equations in which the number of measurements exceed the number of unknowns is given by

$$Y^* = CX^*$$

where

$$Y^* = \begin{bmatrix} Y_1 \\ Y_2 \\ \vdots \\ Y_5 \end{bmatrix}$$

$$C = \begin{bmatrix} h_{11} & h_{21} & 0 & 0 \ldots 0 \\ h_{12} & 0 & h_{22} & \cdot \\ \vdots & \vdots & \vdots & \vdots \\ h_{15} & 0 & 0 & \ldots h_{25} \end{bmatrix}$$

and

$$X^* = \begin{bmatrix} X_1 \\ X_2 \\ \vdots \\ X_5 \end{bmatrix}$$

where $h_{11} = \begin{bmatrix} I_{Ra} & -I_{Rb} & 0 \\ I_{Rb} & I_{Ra} & 0 \\ I_{sa}+I_{Ra} & I_{sb}+I_{Rb} & I_{Rb} \\ I_{sb}+I_{Rb} & I_{sa}+I_{Ra} & I_{Ra} \end{bmatrix}_i$

and

$$h_{21} = \begin{bmatrix} 0 & R_m & -X_m & \\ 0 & X_m & R_m & \\ I_{Ra} & R_m+R_R & -X_m & -X_R \\ I_{Rb} & X_m+X_R & R_m + R_R & \end{bmatrix}_i$$

for $i = 1, 2, \ldots, 5$.

An iterative solution to the concatenated measurement equation is obtained as follows.

Initial estimates of C and X^* are obtained based on the

no load test data, the load test data, and knowledge of the range of values of machine parameters associated with machines of this type and rating. Using a digital computer program, a correction to the states is obtained by calculating the pseudo inverse of C, viz,

$$C^{+} = (C'C)^{-1}C'.$$

The correction to the state vector at each iteration is given by

$$\Delta X^{*} = C^{+} (Y^{*} - \hat{Y}^{*})$$

where $\hat{Y}^{*}$ is the value of the measurement based on the values of the state calculated on the previous iteration. The state vector is corrected by

$$X = X^{*}_{k-1} + \Delta X^{*}.$$

If the initial guess is sufficiently close to the values that solve the system of equations, the process is continued until the correction to the state ΔX^{*} becomes negligibly small.

Results obtained using this procedure based on five sets of load test data are

$$R_m = 0.39 \text{ ohms}$$

$$X_m = 8.72 \text{ ohms}$$

$$X_R = 0.17 \text{ ohms}$$

Values of rotor resistance R_R which is a function slip are shown in the following table

slip (per unit)	$\frac{R_R}{s}$ ohms	R_R' ohms
0.0833	3.088	0.257
0.0633	3.558	0.225
0.0500	4.383	0.2192
0.0233	15.23	0.355
0.0267	10.90	0.291

The average value of the rotor resistance is

$$R_R' = 0.269 \text{ ohms.}$$

The equivalent circuit parameters are obtained by straightforward algebraic manipulation and are given by

$R_s = 0.11$ ohms

$R_\phi = 195$ ohms

$X_\phi = 8.74$ ohms

$X_s = 0.71$ ohms

$R_R' = 0.269$ ohms

$X_R = 0.17$ ohms.

These values are based on open circuit impedance

$$Z_{oc} = 0.5 + j\ 9.429 \text{ ohms.}$$

Convergence to two decimal places in ΔX^* occurred on the fifth iteration for the particular initial guess used. These data formed the basis for the simulation comparison test discussed in Chapter II.

APPENDIX B

SYSTEM SIMULATION

Introduction

This appendix describes the digital simulation of the system used to obtain the data presented in chapters II and III of the text. The approach to the development of the simulation embodies a number of subroutines, and an overall executive program that calls the subroutines in appropriate sequence. There are two different sample intervals in the program; the continuous dynamic elements are simulated at a much higher rate than the discrete dynamic elements. Parameter value input is accomplished using a common array and variables to be plotted are stored at preselected intervals on a mass storage device. The actual generation of the plots is accomplished using a separate program. In the following sections, an overall flow chart of the simulation is presented and discussed, the inputs required to run the program and the variables stored for plotting are described. Because of the volume of listings and potentially limited interest in the program details, no listings are included; however, a complete listing is available under separate cover in the Department of Electrical and Computer Engineering Library.

Simulation Description

The simulation program flow chart is shown in figure B-1. The data input is accomplished using cards with up

to six data entries per card. In general, the initial conditions are established in the various subroutines the first time the subroutine is called under control of a logical variable. Integration of the continuous dynamic elements is accomplished using a first order predictor and Euler corrector on each integration interval. On the nearest interval to the switching time of the power supply voltage, the gains and control are calculated. The discrete sampletime varies with the fundamental frequency of the voltage waveform but is always associated with 60 degree intervals of the fundamental. At selected times, transfer function pole placement is evaluated as described in chapter III. At preselected intervals, variables to be plotted are stored on a mass storage device. On reaching input value of the maximum simulation time, a check is made to determine if additional data are to be input; if no additional data are present, the program stops. The names and a phrase description of the various routines are shown in Table B-1.

Inputs and Outputs

The simulation inputs are shown in Table B-2. This table indicates the location, quantity, description and units of the variables and parameters required to execute the program. Table B-3 describes the simulation variables that are placed on mass storage for subsequent plotting.

Printed output is obtained at selected time intervals consisting of internal variables which serves as a check on the operation of the program, and the results of the transfer faction evaluation subroutines.

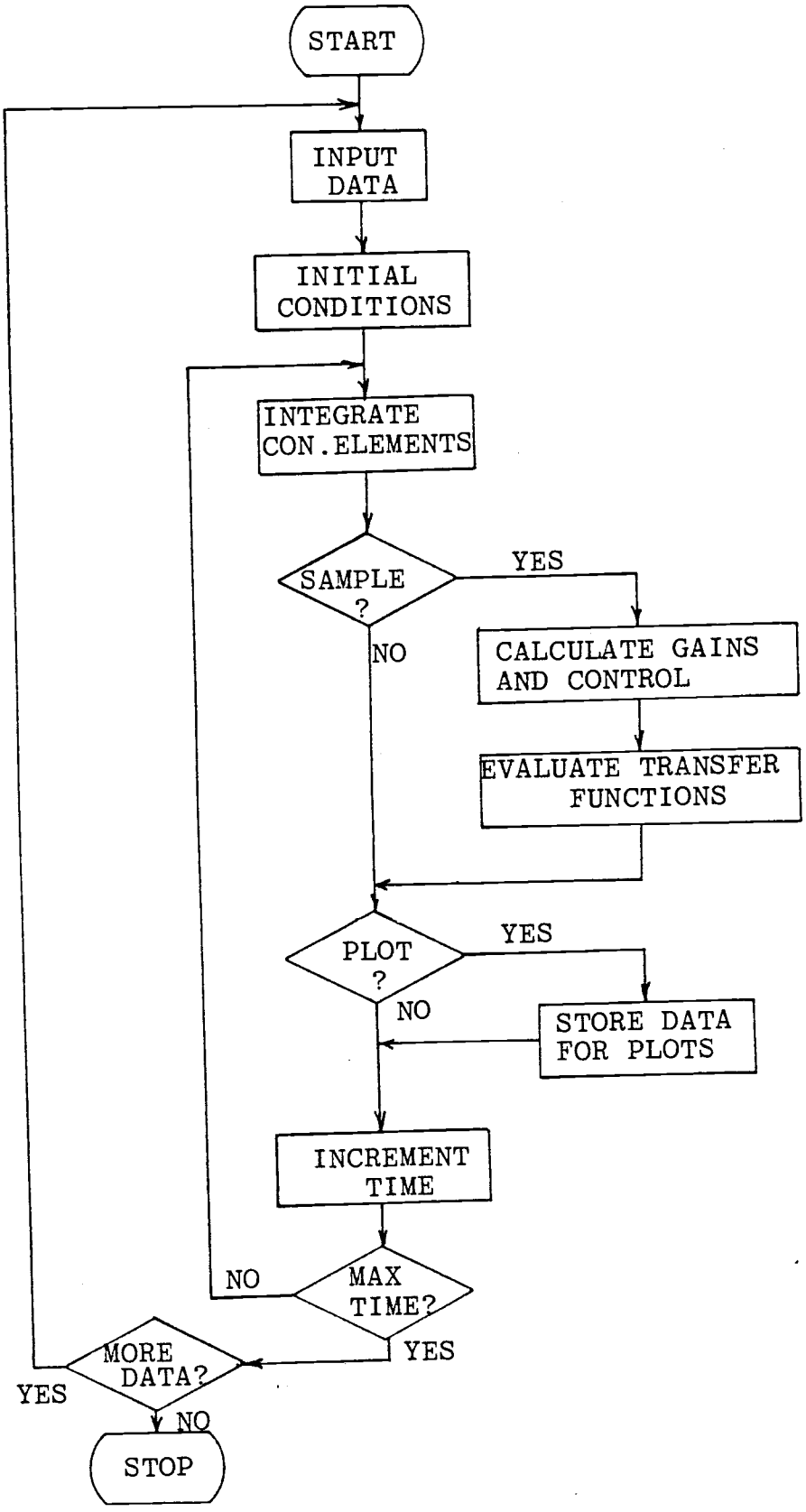

Figure B-1. Simulation Program Flow Chart.

TABLE B-1

SIMULATION ROUTINES

NAME	FUNCTION
SEWER	Overall program control; data input and output
AXI	Adds a unit matrix to a matrix
AXY	Matrix addition
BODE	Evaluates a polynomial ratio in s as a function of frequency and prints the result
BODEZ	Evaluates a polynomial ratio in z as a function of frequency and prints the results
CLOB	Inputs data from cards into specified anay elements, prints the values and controls the number of data sets to be used.
CLOOP	Evaluates closed loop discrete transfer function
CNVRTR	Simulates six-step d.c.-link frequency converter waveform
CONTRL	Calculates system feed-back gains and control vector
CORRl	Euler corrector integration
DERIVF	Evaluates Jacobian matrix for use in calculation of feed-back gains
FLUX	Evaluates nonlinear system state derivative
GAINS	Evaluates discrete Ricatti equation
MINV	Matrix inverter (from IBM Scientific Subroutine Package)
MI3	Closed form three-by-three matrix inverter
MSX	Multiplication of a matrix by a scaler
MXTY	Multiplication of a matrix by the transpose of another matrix

TABLE B-1, cont.

NAME	FUNCTION
MXY	Matrix Multiplication
MXYT	Multiplication of the transpose of a matrix by another matrix
PRED1	First order predictor integration
TRAN	Evaluates discrete state and control transition matrix using exporential approximation
XFN	Evaluates transfer function from system matrix using Leverrier's algorithm
XFNEIG	Evaluates roots of transfer function polynomials--calls BODE, BODEZ and PRQD. PRQD is an IBM Scientific Subroutine Package root finder
ZERO	Sets the elements of a matrix to zero

TABLE B-2

Simulation Input Parameters

LOCATION	QUANTITY	DESCRIPTION	UNITS
1	tmax	Simulation time	s
2	Δt	Continuous dynamic element integration interval	s
3	Δtprint	Print interval	s
4	Δtplot	Plot interval	s
5	Plot flag	Plot if ≥ 0	-
6		not used	
7		↓	-
8	N_g	Number of plot variables	-
9		not used	
10			
11			
12			
13			
14			
15			
16			
17			
18	P	Number of motor poles	-
19	r_s	Stator resistance	ohms
20	r_r	Rotor resistance	ohms
21	X_s	Stator reactance of base frequency	ohms
22	X_m	Magnetizing reactance at base frequency	ohms
23	X_r	Rotor reactance at base frequency	ohms
24		not used	
25		↓	
26	ω_b	Base frequency	r/s
27		not used	
28		↓	
29	h_c	Commanded well head	m
30	q_i	Input and commanded flow	m^3/s
31	k_t	Pump reaction torque coefficient	$N\text{-}m/(r/s)^2$
32	k_h	Pump output head coefficient	$m(r/s)^2$
33	k_f	System friction head coefficient	$m/(m^3/s)$
34	h_s	System static head	m
35	m	System fluid mass	kg

TABLE B-2, cont.

LOCATION	QUANTITY	DESCRIPTION	UNITS
36	k_w	Reciprocal of well area	m^{-2}
37	J	Rotating mass moment of inertia	$kg-m^2$
38	D	Viscous friction coefficient	N-m/(r/s)
39		not used	
40			
41	V_{mc}	Peak amplitude of nominal supply voltage fundamental	V
42	ω_{sc}	Nominal Supply Voltage fundamental frequency	r/s
43	v_{mmax}	Maximum value of supply voltage	V
44	ω_{smax}	Maximum value of supply frequency	r/s
45		not used	
46			
47			
48			
49			
50	ω_c	Commanded shaft frequency	r/s
51	r_{11}	Voltage weighting	-
52	r_{22}	frequency weighting	-
53			-
54	q_{11}	Current weighting	-
55	q_{22}	Current weighting	-
56	q_{33}	Current weighting	-
57	q_{44}	Current weighting	-
58	q_{55}	Shaft frequency error weighting	-
59	q_{66}	Flow error weighting	-
60	q_{77}	Well head error weighting	-
61		not used	
.			
.			
.			
100			

TABLE B-3

VARIABLES STORED FOR PLOTTING

LOCATION	QUANTITY	DESCRIPTION	UNITS
1	t	Time	s
2	v_a	Phase A stater voltage	V
3	v_b	Phase B stator voltage	V
4	v_c	Phase C stator voltage	V
5	i_{sa}	Phase A stator current	A
6	i_{sb}	Phase B stator current	A
7	i_{sc}	Phase C stator current	A
8	t_e	Electromagnetic torque	N-m
9	ω_m	Shaft frequency	r/s
10	q_p	Pump output flow	m^3/s
11	h_w	Well head	m
12	q_i	Input flow	m^3/s
13	ω_s	Supply fundamental frequency	r/s
14	V_m	Peak supply voltage fundamental	V
15	i_{ra}	Phase A rotor current	A
16	i_{rb}	Phase B rotor current	A
17	i_{rc}	Phase C rotor current	A